2012

Mechanical AGN feedback: controlling the thermodynamical evolution of elliptical galaxies

M. Gaspari
University of Bologna, massimo.gaspari4@unibo.it

F. Brighenti
University of Bologna

P. Temi
NASA/Ames Research Center, ptemi@mail.arc.nasa.gov

Monthly Notices
of the
ROYAL ASTRONOMICAL SOCIETY

Mon. Not. R. Astron. Soc. **424,** 190–209 (2012) doi:10.1111/j.1365-2966.2012.21183.x

Mechanical AGN feedback: controlling the thermodynamical evolution of elliptical galaxies

M. Gaspari,[1⋆] F. Brighenti[1] and P. Temi[2]

[1]*Astronomy Department, University of Bologna, Via Ranzani 1, 40127 Bologna, Italy*
[2]*Astrophysics Branch, NASA/Ames Research Center, MS 245-6, Moffett Field, CA 94035, USA*

Accepted 2012 April 25. Received 2012 April 23; in original form 2012 February 27

ABSTRACT

A fundamental gap in the current understanding of galaxies concerns the thermodynamical evolution of ordinary, baryonic matter. On the one hand, radiative emission drastically decreases the thermal energy content of the interstellar plasma (ISM), inducing a slow cooling flow towards the centre. On the other hand, the active galactic nucleus (AGN) struggles to prevent the runaway cooling catastrophe, injecting huge amount of energy into the ISM. The present study intends to investigate thoroughly the role of mechanical AGN feedback in (isolated or massive) elliptical galaxies, extending and completing the mass range of tested cosmic environments. Our previously successful feedback models in galaxy clusters and groups demonstrated that AGN outflows, self-regulated by cold gas accretion, are able to quench the cooling flow properly without destroying the cool core. Via three-dimensional hydrodynamic simulations (FLASH 3.3), also including stellar evolution, we show that massive mechanical AGN outflows can indeed solve the cooling-flow problem for the entire life of the galaxy, at the same time reproducing typical observational features and constraints such as buoyant underdense bubbles, elliptical shock cocoons, sonic ripples, dredge-up of metals, subsonic turbulence and extended filamentary or nuclear cold gas. In order to avoid overheating and totally emptying the isolated galaxy, the frequent mechanical AGN feedback should be less powerful and efficient ($\epsilon \sim 10^{-4}$) compared with the heating required for more massive and bound ellipticals surrounded by the intragroup medium ($\epsilon \sim 10^{-3}$).

Key words: hydrodynamics – galaxies: active – intergalactic medium – galaxies: ISM – galaxies: jets – X-rays: galaxies.

1 INTRODUCTION

The present paper is the third in a series aimed at investigating how massive black holes (BHs) control the thermal and dynamical evolution of the gaseous component of galaxies, groups and clusters. The focus of this investigation is the effect of active galactic nucleus (AGN) feedback on the interstellar medium (ISM) of isolated and massive elliptical galaxies.

The key role of AGN outbursts in sterilizing the parent galaxy – quenching star formation and gas cooling – has become obvious in the last decade. The need for sustained gas heating in a range of astronomical systems comes from both observations and theory. High spatial resolution X-ray and radio images of clusters, groups and elliptical galaxies reveal a clear connection between nuclear activity and large-scale disturbances in the hot gas, such as X-ray cavities, which are often filled with radio emission (e.g. Churazov et al. 2000; Diehl & Statler 2008a; Dunn et al. 2010b; Giacintucci et al. 2011), and shocks (Baldi et al. 2009). These features are thought to be the manifestation of the heating process necessary to prevent the excessive gas cooling predicted by the classic cooling-flow theory (Fabian 1994; Mathews & Brighenti 2003). X-ray and UV spectroscopy indeed indicates cooling rates at least one order of magnitude lower than simple expectations, in both galaxies and clusters/groups – this is the so-called *cooling-flow problem* (Bregman, Miller & Irwin 2001; Oegerle & Hill 2001; Peterson et al. 2001, 2003; Xu et al. 2002; Tamura et al. 2003; Bregman et al. 2005, 2006). Excellent reviews on this subject are provided by Peterson & Fabian (2006), McNamara & Nulsen (2007) and Böhringer & Werner (2010).

Another piece of evidence for reduced cooling rates comes from the lack of significant star formation in most massive elliptical galaxies (Ferreras & Silk 2000; Trager et al. 2000; Graves, Faber & Schiavon 2009; Jeong et al. 2009), which are typically located in the quiescent part of the infrared colour–colour diagram (Temi, Brighenti & Mathews 2009).

The problem of ISM heating and the related absence of cold gas in elliptical galaxies is long-lasting. This was investigated forty

⋆E-mail: massimo.gaspari4@unibo.it

years ago by Mathews & Baker (1971) in a seminal paper to explain the dearth of cold ISM in typical ellipticals. They proposed that Type Ia supernova (SNIa) explosions heat and eject the ISM, which is continuously supplied by stellar winds from evolving stars. Subsequent investigations (MacDonald & Bailey 1981; Mathews & Loewenstein 1986; Loewenstein & Mathews 1987; Ciotti et al. 1991; David, Forman & Jones 1991) have analysed in depth the secular evolution of the ISM in isolated ellipticals. SNIa heating is indeed able to prevent gas cooling and drive global winds in small or intermediate ellipticals but not in massive galaxies, which usually reside at the centre of a massive dark halo. These systems necessitate a different energy source.

Furthermore, galaxy formation theory requires a mechanism to reduce the star formation in massive galaxies substantially in order to agree with the observed sharp cut-off of the luminosity function at the high-mass end (Benson et al. 2003; Balogh et al. 2006; Croton et al. 2006; Cattaneo et al. 2009), although ellipticals at the centre of cool-core systems sometimes show significant star-formation rates (O'Dea et al. 2008). It is now clear that supernova heating alone is insufficient to prevent gas from cooling and forming stars (Tornatore et al. 2003; Piontek & Steinmetz 2011). Thus, the black hole at the centre of a massive galaxy becomes the natural suspect for providing the required feedback heating (Binney & Tabor 1995; Churazov et al. 2002).

From an energetic point of view, AGNs are able to satisfy the galaxy or cluster heating demand. For a typical black hole mass of $M_{\rm BH} \approx 10^9\,{\rm M}_\odot$ (Ferrarese & Merritt 2000; Gebhardt et al. 2000[1]), an amount of energy $E_{\rm BH} \approx 0.1\,M_{\rm BH}c^2 \approx 2 \times 10^{62}$ erg could in principle be injected into the surrounding gas. This is a sizeable fraction of all the energy radiated away by the intracluster medium (ICM) during a massive cluster lifetime, and is significantly larger than the binding energy of the ISM in a typical elliptical galaxy or group. For example, the gas binding energy for the massive, X-ray-bright group NGC 5044 is $\approx 9 \times 10^{61}$ erg (Mathews et al. 2005).

Many fundamental questions about the physics of AGN feedback, however, remain unanswered (see also Ostriker et al. 2010). A key issue is to identify the physical process through which the AGN interacts with the surrounding gas. Several mechanisms have been proposed and investigated numerically, including radiative heating by quasars (Ciotti & Ostriker 1997), cavities generated through the injection of thermal energy or cosmic rays (Dalla Vecchia et al. 2004; Brüggen, Ruszkowski & Hallman 2005; Mathews & Brighenti 2008; Mathews 2009; Guo & Mathews 2010), or bipolar mechanical outflows/jets (Omma et al. 2004; Soker & Pizzolato 2005; Zanni et al. 2005; Brighenti & Mathews 2006; Vernaleo & Reynolds 2006; Brüggen et al. 2007; Gaspari et al. 2009, 2011a,b; Gaspari, Ruszkowski & Sharma 2012).

In low-redshift systems it seems likely that massive black holes mostly accrete mass and return energy in a radiatively inefficient way (Fabian & Rees 1995; Loewenstein et al. 2001; Di Matteo et al. 2003; Taylor et al. 2006). Thus, while luminous quasars might have been an important source of heating at high redshift, with the peak of the QSO distribution at $z \sim 2$ (Nesvadba et al. 2008; Moe et al. 2009; Dunn et al. 2010a), observations point to advection-dominated accretion flow (ADAF) like systems as a primary source of local AGN feedback. These accretors naturally generate powerful outflows (Narayan & McClintock 2008 and references therein).

Recent X-ray and radio observations (see the reviews by McNamara & Nulsen 2007; Gitti, Brighenti & McNamara 2012) provide crucial guidance on how to narrow down the range of possible heating scenarios. The common presence of radio-filled X-ray cavities, ellipsoidal weak shocks and metal (iron) enhancements along the radio jet path (e.g. Gitti et al. 2010; Kirkpatrick, McNamara & Cavagnolo 2011; Randall et al. 2011) strongly suggests that local AGNs introduce energy directionally and in mechanical form, likely as bipolar massive outflows or jets.

For this reason, in Gaspari et al. (2011a,b, hereafter G11a,b) we tested a variety of outflow models in clusters and groups in order to verify whether this mechanical feedback is able to quench cooling without overheating the core, an often unwelcome byproduct of central energy injection (Brighenti & Mathews 2002, 2003, 2006). We showed that massive, subrelativistic outflows are indeed a viable mechanism to solve the cooling-flow problem in clusters and groups. In lighter systems the AGN feedback must, however, be more gentle and continuous or, in other words, in massive clusters possible quasi-continuous low-power activity must be intermixed with sporadic powerful events.

In the present work we study how AGN feedback self-regulates in a galactic environment and test the models against several observational constraints. Massive elliptical galaxies are in fact important laboratories in which to study the AGN feedback process in the local Universe. Their ISM shines in the X-ray and many giant ellipticals are relatively nearby, within a distance of ∼15–30 Mpc, a valuable virtue compared with X-ray-bright but distant massive clusters. The relative proximity thus allows the investigation of a region closer to the AGN, where the feedback engine might manifest itself in a clearer way.

In Section 2, we present our theoretical modelling and the details of the numerical methods. We adopt a simple recipe to activate the outflows, based on gas cooling near the central black hole. We discuss in Section 2.1.1 why it is not feasible to investigate the accretion and the outflow generation processes with appropriate accuracy. We instead turn our attention to the effect of the outflows on large scales. We analyse the observable consequences of the assumed feedback scenario on the environment of an isolated elliptical (Section 3) and a galaxy with circumgalactic gas (Section 4). In Section 5, we discuss the key features of the results presented in this work and summarize the effects of mechanical AGN feedback on every scale, from galaxies to massive clusters.

2 THEORETICAL AND NUMERICAL SET-UP

2.1 AGN feedback

2.1.1 What is the accretion rate?

As remarked in the Introduction, massive black holes in nearby X-ray-bright ellipticals likely accrete gas through a radiatively inefficient mechanism. ADAF models naturally predict outflows and jets (Narayan & McClintock 2008), which might provide the mechanical feedback we study in the present article.

Our feedback scheme assumes that the black hole reaction is proportional to the accretion rate (Section 2.1.2). This simple conjecture leads, however, to a substantial difficulty in building a self-consistent model, i.e. properly estimating the BH accretion rate. This is such a complex problem that we should not be ashamed to accept our ignorance. We give below some reasons why the

[1] The most massive BHs at the centre of the brightest clusters can even be an order of magnitude heavier, like the BH in NCG 4889 with $M_{\rm BH} \sim 2 \times 10^{10}\,{\rm M}_\odot$ (McConnell et al. 2011).

accretion rate (and the BH growth) cannot be investigated in depth within the frame of our models and must therefore be estimated with some subgrid scheme, which usually depends on the uncertain gas properties in the nuclear region. Because the simulated ISM in the central few hundred pc is quite different from that of real ellipticals, our calculated accretion rate should not be trusted with high confidence. We suspect that this is true for most numerical works on AGN feedback, either in galaxies or clusters. Specifically, the motivations that lead to a rather uncertain accretion rate are the following.

(i) In order to model the three-dimensional accretion flow self-consistently, using magnetohydrodynamics, the necessary condition is to resolve numerically a region with size of a few Schwarzschild radii, $R_{\rm S} \approx 3 \times 10^{14}(M/10^9\,{\rm M}_\odot)\,{\rm cm} \approx 10^{-5} R_{\rm B}$ (where $R_{\rm B}$ is the usual Bondi radius). This is currently not feasible for three-dimensional (3D) simulations aimed to investigate galactic-scale flows. Because the direct calculation is impractical, we are left to rely on a subgrid prescription to estimate the accretion rate. However, this is a formidable task; the exact quantity of material that is considered 'accreted' must be used with great caution and only as a rough approximation.

(ii) Many studies – including ours (G11a,b) – use the Bondi (1952) theory to estimate the instantaneous mass accretion rate on to the BH (Springel, Di Matteo & Hernquist 2005; Cattaneo & Teyssier 2007; Sijacki et al. 2007; Puchwein, Sijacki & Springel 2008; Booth & Schaye 2009; Dubois et al. 2010). In order to make results compatible with observations, the Bondi accretion rate is often artificially and arbitrarily boosted by a factor of $\sim$100 (see Booth & Schaye 2009 for a related discussion). While this is a convenient parametrization, it seems unsafe to rely on it for a realistic representation of the accretion process. Beside complications such as turbulence, rotation and magnetic fields (see Krumholz, McKee & Klein 2005, 2006; Igumenshchev 2006; Mościbrodzka & Proga 2008, 2009; Narayan & Fabian 2011), which can easily change the classic accretion rate by a factor of a few, we believe that cooling (and heating) make the Bondi assumption particularly hazardous. The central ISM can be prone to thermal instabilities, which can drastically change the nature of the accretion process (Pizzolato & Soker 2005; Gaspari et al. 2012; McCourt et al. 2012; Sharma et al. 2012). In fact, in the presence of a classical cooling flow the mass inflow rate at some small radius is determined by the gas cooling process rather than the BH gravity. Thus, we expect $\dot{M}_{\rm BH} \approx 0.1$–$1\,{\rm M}_\odot\,{\rm yr}^{-1}$ for an isolated elliptical galaxy. Accretion scenarios suggested by King & Pringle (2007) and Pope (2007, 2009) also differ significantly from the Bondi prediction.

The common assumption in numerical models is to take as Bondi boundary conditions some average of density and temperature within a radius larger than $R_{\rm B}$, usually a simulated region filled with smooth hot gas. However, the real ISM at the fiducial Bondi radius for the hot gas ($\approx$50 pc) is often comprised of a multiphase, dusty $\sim 10^4$ K gas (Heckman et al. 1989; Shields 1991; Buson et al. 1993; Goudfrooij et al. 1994; Macchetto et al. 1996; Ferrari et al. 1999; Martel et al. 2000; Tran et al. 2001; Colbert, Mulchaey & Zabludoff 2001; Verdoes Kleijn et al. 2002), which can be both dynamically relaxed or in chaotic motion (Caon, Macchetto & Pastoriza 2000; Sarzi et al. 2006, 2010). This warm gas is likely intermixed with hot ISM, and the interaction between the two phases is poorly understood. With such complex gas conditions, it is difficult to estimate the accretion rate. With one-dimensional (1D) or two-dimensional (2D) simulations it is relatively easy to resolve the Bondi radius in galactic flows (Ciotti & Ostriker 1997; Brighenti & Mathews 1999; Quataert & Narayan 2000; Novak, Ostriker & Ciotti 2011), yet the necessarily simplified gas physics adopted and the limits imposed by the geometry prevent these models from catching the complexity of the ISM near the black hole.

Because of these (not easily quantifiable) uncertainties we prefer not to assume any sophisticated subgrid modelling for the accretion process.

(iii) Finally, the assumptions made for stellar source terms (smooth injection of mass and energy from evolved stars and SNIa), described in Section 2.2.1 (see also Mathews & Baker 1971; Loewenstein & Mathews 1987; Mathews & Brighenti 2003), clearly break down within the galactic core. A mature SNIa remnant would have a size of $\approx$50 pc if the external medium has a number density of $\sim 0.1\,{\rm cm}^{-1}$ and a temperature $\sim 10^7$ K, comparable with the galactic core radius. Stellar winds from orbiting stars likely generate long tails of warm gas, several tens of pc in size (Mathews 1990; Parriott & Bregman 2008; Bregman & Parriott 2009), giving rise to inhomogeneities. The stellar material can indeed help to explain the ubiquitous presence of emission-line gas at the centre of early-type galaxies (Mathews & Brighenti 2003). These intrinsic limitations, along with the lack of merging as a possible source of gas, hamper a proper modelling of the ISM in the central $\approx$100–200 pc.

For all the previous reasons, we believe that it is futile to investigate the details of BH accretion history in the present work. Therefore, we realistically limit the goal of our study to the effects of (large-scale) outflows on ISM evolution.

2.1.2 Self-regulated mechanical outflows

Encouraged by the results in G11a and G11b for clusters and groups, we consider here subrelativistic collimated outflows as the main ingredient of the AGN mechanical feedback in elliptical galaxies. In considering massive slow outflows, we are implicitly assuming that the relativistic jet entrains some ISM mass (the active mass $M_{\rm act}$, defined below) or perhaps that a wind originates from the accretion disc (Crenshaw, Kraemer & George 2003; Morganti et al. 2007; Nesvadba et al. 2008; Cappi et al. 2009; Cappi, Giustini & Tombesi 2011; Tombesi et al. 2010a,b, 2012; see also the references in G11a,b). Moreover, radio jets are highly relativistic on a pc scale, but rapidly decrease to subrelativistic velocities within a few kpc from the black hole (Giovannini 2004).

In G11b we showed that, on galaxy group scales, the self-regulation imposed by cold gas accretion tends to generate a quasi-continuous, gentle feedback, qualitatively similar to that expected for boosted (by a factor of $\sim$100) Bondi accretion. However, on top of this low-level AGN activity, several powerful outbursts can occur, which produce visible cavities and shocks, a desirable feature of those models. Therefore, in the present work on elliptical galaxies we preferred to adopt a cold feedback mechanism (see also Pizzolato & Soker 2005), where the assumed accretion rate is linked to the cooled gas in a given central region. As pointed out in Section 2.1.1, there are several reasons to believe that a purely Bondi accretion scenario (that is, the hot feedback mode) is inappropriate.

We slightly improved the feedback self-regulation mechanism in comparison with G11a,b. The radius of the region used to estimate the accreted cold gas – usually several kpc – was rather arbitrary, and we assumed that the jet is instantaneously triggered only by the gas cooled near the centre of the system. This length-scale was reasonable because almost all the cooling occurred inside the chosen radius.

In order to eliminate this parameter, we adopt here the physical assumption that the cooled gas (dropped out at radius $r_{\rm i}$; Section 2.3.2) goes into free fall and accretes on to the black hole in a free-fall time, given by

$$t_{\rm ff} = \int_{r_{\rm i}}^{0} \frac{{\rm d}r}{\sqrt{2\,|\phi(r) - \phi(r_{\rm i})|}}\,, \quad (1)$$

where ϕ is the gravitational potential (associated with the stellar and dark matter mass distribution). We also impose that the infalling gas must have a low angular momentum, i.e. less than $v_{\rm c}(\Delta r)\,\Delta r$ (circular velocity times the minimum radial grid size). Most of the cooled gas tends nevertheless to have negligible angular momentum (see also Pizzolato & Soker 2010). This new method does not require the fixed radius used in G11a,b, since the accretion is no more instantaneous while it is set by the free-fall time delay; the latter is dependent on where cold clouds condense locally out of the hot phase.

The cold mass reaching the centre at a given time, $\Delta M_{\rm c,tot}$, triggers an outflow with kinetic energy given by

$$\Delta E_{\rm jet} = \epsilon\,\Delta M_{\rm c,tot}\,c^2, \quad (2)$$

where ϵ is the parametrized mechanical efficiency of the feedback. It is likely that the efficiency depends on the ratio between the actual accretion rate and the Eddington rate, $\dot{M}_{\rm Edd} \approx 22\,(M_{\rm BH}/10^9\,{\rm M}_\odot)\,{\rm M}_\odot\,{\rm yr}^{-1}$ (Churazov et al. 2005; Merloni & Heinz 2008). However, given the uncertainties in estimating the accretion rate, we prefer to assume a constant efficiency.

This kinetic energy (and the associated momentum) is given to the gas located in a small region at the centre of the grid (the 'active' jet region), the size of which is usually[2] $\Delta R \times \Delta z = 2 \times 1$ cells (about 300 pc wide, 150 pc high), containing some hot gas mass $M_{\rm act}$. The outflow velocity was retrieved as usual (G11a,b), imposing

$$\frac{1}{2} M_{\rm act} v_{\rm jet}^2 = \Delta E_{\rm jet}. \quad (3)$$

2.2 Galaxy models

2.2.1 Isolated elliptical

In this section we describe the modelling of the elliptical galaxy, providing the initial conditions for the simulations. We model a massive elliptical galaxy with a de Vaucouleurs' stellar density profile (approximated as in Mellier & Mathez 1987), with effective radius $r_{\rm eff} = 8.5$ kpc and total stellar mass $M_* = 7 \times 10^{11}\,{\rm M}_\odot$. Assuming a stellar mass-to-light ratio of 8 (in the B band), appropriate for an old stellar population, the resulting luminosity is $L_B = 8.75 \times 10^{10}\,{\rm L}_\odot$. Thus, our model represents a typical elliptical galaxy similar to NGC 4649, NGC 4472 and many others in the local Universe, albeit without the intragroup medium. The dark matter is modelled as a Navarro, Frenk & White (NFW) halo (Navarro, Frenk & White 1996) with virial mass $M_{\rm vir} = 4 \times 10^{13}\,{\rm M}_\odot$ and a concentration $c = 8.8$ (Bullock et al. 2001; Humphrey et al. 2006).

Several ingredients characterize the stellar mass and energy sources (stellar winds and SNIa). The specific stellar-wind mass return rate is assumed to be $\alpha_* = 4.7 \times 10^{-20}(t/t_{\rm n})^{-1.3}\,{\rm s}^{-1}$, where $t_{\rm n} = 13$ Gyr is the galaxy age (results are not sensitive to the adopted $t_{\rm n}$). This formula is a good approximation for a single stellar population older than 100 Myr. The SNIa mass return rate depends on the SNIa rate, $r_{\rm Ia} = 0.06\,(t/t_n)^{-1.1}$ SNu (Cappellaro, Evans & Turatto 1999; Greggio 2005; Mannucci et al. 2005). With the chosen SNIa rate, the specific SNIa mass return rate is $\alpha_{\rm Ia} = 3.17 \times 10^{-20}\,r_{\rm Ia}(t)(M_{\rm ej}/{\rm M}_\odot)/(M_*/L_B)$, where $M_{\rm ej} = 1.4\,{\rm M}_\odot$ is the ejecta mass of a SNIa and $M_*/L_B = 8$ is the stellar mass-to-light ratio in the B band. The adopted $r_{\rm Ia}$ results in gas abundances consistent with observations (Humphrey & Buote 2006).

The energy injection associated with stellar winds and SNIa is treated as outlined in Mathews & Brighenti (2003). The stellar velocity dispersion, which determines the temperature of the injected wind gas, is calculated by solving the Jeans equation for a spherically symmetric, isotropic stellar system. Fortunately, the stellar wind heating does not have a large impact on the flow and it is not necessary to calculate $\sigma_*(r)$ using more sophisticated dynamical models.

Concerning the gaseous component, we decided to simulate two kinds of systems. In the first one, indicated as an 'isolated galaxy', the ISM is produced by internal processes alone (stellar mass loss and SNIa ejecta). Although the hot ISM of massive, X-ray-bright ellipticals cannot be realistically explained without a circumgalactic gas component (Brighenti & Mathews 1998, 1999), we decided to use this approach for its simplicity and to allow direct comparison with previous calculations of hot gas flows in ellipticals (e.g. Loewenstein & Mathews 1987; Ciotti et al. 1991; Ciotti & Ostriker 1997). Within $\sim r_{\rm eff}$, most of the ISM is indeed likely to come from stellar mass loss (Brighenti & Mathews 1999). Thus, the terminology 'isolated galaxy' does not refer to the presence of other (large) galaxies nearby, but the fact that the ISM is not contaminated by the group or cluster gas.

The simulations of an isolated galaxy start at cosmic time $t = 1$ Gyr with the galaxy essentially devoid of gas, conforming to the usual assumption that the gas has been cleared by a SNII-driven wind. The ISM is then gradually supplied by the stars. After a few 10^8 yr, the system loses its memory of the initial conditions and, if not heated, approaches a quasi-steady state, with secular changes controlled by the slow variation of the stellar-mass return rate (Loewenstein & Mathews 1987; Ciotti et al. 1991). The simulations are evolved to a final time of 13 Gyr.

2.2.2 Elliptical with circumgalactic gas

In the second class of models, more realistic and appropriate for a detailed comparison with well-observed galaxies, we take into account the presence of circumgalactic gas (CGG). Many of the famous X-ray ellipticals belong to this breed. A distinctive characteristic of classic cooling-flow models with CGG is the presence, often observed in real systems, of a relatively broad cool core, in perfect analogy with galaxy clusters (Brighenti & Mathews 1998, 1999; Humphrey et al. 2006; Diehl & Statler 2008b). The separation between galaxies with CGG and galaxy groups is largely semantic, so these models are tightly linked to those calculated in G11b. However, here we focus mainly on the region close to the galaxy ($r \lesssim r_{\rm eff}$). At variance with G11b, we used an improved feedback scheme (Section 2.1.2) and adopted a significantly higher numerical resolution.

The galaxy parameters are chosen to agree with NGC 5044, an X-ray-bright galaxy in the centre of the homonymous group with $r_{\rm eff} = 10$ kpc, $M_* = 3.4 \times 10^{11}\,{\rm M}_\odot$ and $M_*/L_B = 7.5$ (see Buote, Brighenti & Mathews 2004). In these simulations we use the observed $T(r)$ and $n(r)$ profiles (David et al. 1994; Buote et al. 2003;

[2] A slightly smaller or larger active region does not drastically alter the global evolution (see G11a,b). The same is true if we inject the energy from the internal boundaries of the grid.

see the dotted lines in Fig. 4 later) to retrieve the total gravitational potential under the assumption of hydrostatic equilibrium.

We run the CGG models for 7 Gyr. As emphasized in G11a, it is crucial to check the long-term behaviour of a heated model in order to assess its merit. Unfortunately, short-term simulations can in fact return misleading results on a particular feedback model as a solution of the cooling-flow problem.

2.3 Numerical techniques

2.3.1 Code set-up

As in G11a,b, we have used a substantially modified version of the 3D hydrodynamic code FLASH 3.3 (Fryxell et al. 2000). The main advantages include the adaptive mesh refinement (AMR) block structure, suited for a very efficient scalability through the message-passing interface (MPI). The simulations were carried out on the parallel high-performance clusters SP6 (CINECA) and Pleiades (NASA). We employed the Piecewise Parabolic Method (PPM) split scheme to treat the transport terms in the conservation equations (in principle third-order accurate). A full description of the hydrodynamic equations can be found in G11a,b, with the additional source terms representing AGN feedback, radiative cooling and stellar winds plus SNIa.

The computational rectangular 3D box in almost every model extends up to 150 kpc. We have simulated the $z > 0$ half-space with a reflection boundary condition at $z = 0$, elsewhere setting the usual outflow condition with inflow prohibited. Despite the AMR capability of FLASH, we have decided to use a number of concentric fixed grids in Cartesian coordinates. This ensures a proper resolution of the waves and cavities generated in the core by the AGN outflows. We employed a set of 7 grid levels (basic blocks of $16 \times 16 \times 8$ points), with zone linear size doubling between adjacent levels. The most distant regions from the centre are covered by at least level 4. The finest, inner grid (level 7) has a resolution of $\Delta x = \Delta y = \Delta z =$ 146 pc for the isolated galaxy models and covers a spherical region of $\sim$8 kpc in radius. For the simulations with circumgalactic gas, we were forced to lower the resolution to save computational time: $\Delta x = 293$ pc (the inner grid covers $r \sim 16$ kpc); the box is instead four times bigger (8 levels). In general, grids of every level extend radially for about 55 cells. This is arguably the best way to cover very large spatial scales (hundreds of pc up to hundreds of kpc) and at the same time integrate the system for several Gyr.

2.3.2 Radiative cooling

Radiative cooling is a necessary ingredient for studying the cooling-flow problem. We adopt the cooling function by Sutherland & Dopita (1993), dependent on gas temperature and metallicity, $\Lambda(T, Z)$, for a fully ionized plasma. The iron abundance is consistently calculated by solving a passive advection equation for the iron density, with the appropriate sources representing the injection of metals by stellar winds and SNIa (Mathews & Brighenti 2003). We assume that the abundance of all heavy elements in solar units is the same as the iron one. Although this is not strictly true, it has a negligible effect on the cooling process.

We handle the gas cooling at very low temperatures numerically by using a drop-out (mass-sink) term: $-q(T)\rho/t_{\rm cool}$. This is a convenient scheme to remove cold gas from the numerical grid without altering the calculated cooling rate (see G11a for more details).

The numerical implementation has been improved. As is commonly done, we use the splitting method for adding the source/sink terms, i.e. first we solve the standard hydro-equations and then, adopting the updated flow variables, integrate the ordinary differential equation (ODE) associated with the source term. The ODE related to cooling is solved through a second-order Runge–Kutta explicit method. Expanding the cooling time $t_{\rm cool} = 2.5\, nk_{\rm b}T/n_{\rm e}n_{\rm i}\,\Lambda(T, Z)$ and centring the variables leads to the the following discretization for the drop-out ODE:

$$\rho^{\rm n+1} = \rho^{\rm n}\left(1 + \frac{\mu}{2.5\,k_{\rm b}\mu_{\rm e}\mu_{\rm i}m_{\rm p}}\frac{q^{\rm n+1/2}\,\Lambda^{\rm n+1/2}\rho^{\rm n}}{T^{\rm n+1/2}}\,\Delta t\right)^{-1}, \qquad (4)$$

where the indexes refer to the temporal states, Δt is the time-step and the molecular weight per particle, electron and ion are $\mu \sim 0.62$, $\mu_{\rm e} \sim 1.18$ and $\mu_{\rm i} \sim 1.30$, respectively; $T^{n+1/2}$ is conveniently provided by the previous Runge–Kutta mid-point estimate. The functional form of $q = 2\exp[-(T/T_{\rm c})^2]$ ensures that the gas is considered cold and dropped out of the flow as soon as it approaches $T_{\rm c}$. Setting $T_{\rm c} = 2 \times 10^4$ K prevents the formation of very cold clumps in the flow, the physical evolution of which cannot be easily followed by the present computations. It also has the benefit of preventing the drastic decrease of the time-step. Lowering $T_{\rm c}$ permits one to follow the formation of local thermal instabilities better; nevertheless, the global evolution of the cold gas and associated feedback is essentially the same on long time-scales (see Gaspari et al. 2012).

The drop-out term, like any source step, has a time-limiter condition associated. Using the drop-out ODE equation, we find that the relative density decrement, $D = 1 - \rho^{n+1}/\rho^n$, is linked to the following time-scale: $t_{\rm drop} = [D/q(1 - D)]\,t_{\rm cool}$. It is evident that the drop-out limiter is tightly correlated with the cooling limiter $\eta t_{\rm cool}$ (with $\eta < 1$). Limiting the variation of internal energy has the consequence of directly reducing the dropped mass, quantitatively: $D = \eta\, q/(1 + \eta\, q)$. In order to couple the hydro-solver smoothly to the sink terms, a reasonable limiter is $\eta = 0.4$; since the maximum q value can be 2, the drop-out decrement will never exceed $\approx$45 per cent per time-step (it is usually much lower).

3 RESULTS: ISOLATED GALAXY

In Section 3 we report the results for models in which the ISM is produced only by mass loss of the galactic stellar population. We explore the effect of mechanical feedback by varying the key parameter, the efficiency ϵ (see Table 1). In order to solve the cooling-flow problem, AGN outflows must quench the cooling flow without overheating the ISM in a drastic way. The former request is easy to satisfy, if the feedback is energetic enough. The simultaneous fulfilment of the two conditions above is, however, complicated and often requires an unpleasant fine tuning of the heating parameters (Brighenti & Mathews 2002, 2003). Successful feedback also needs to reproduce other observational features, such as cavities, shocks, turbulence, multiphase gas and metal dredge-up.

Table 1. Properties of the most relevant simulations.

Model	Feedback	Efficiency (ϵ)	Notes
iso-CF	no AGN heating	–	isolated
cgg-CF	no AGN heating	–	CGG
iso-1em4	cold	10^{-4}	isolated
iso-3em4	cold	3.3×10^{-4}	isolated
iso-1em3	cold	10^{-3}	isolated
cgg-8em4	cold	8×10^{-4}	CGG

3.1 Pure cooling flow

In Fig. 1 we show the relevant global quantities that characterize a pure cooling-flow model, with AGN heating switched off and the heating provided mainly by the SNIa. This is a classic result: the densest gas loses thermal pressure support due to radiative losses, inducing a slow subsonic inflow ($v_r \lesssim 50\,\mathrm{km\,s^{-1}}$) that further increases the plasma emissivity (a detailed discussion can be found in Mathews & Brighenti 2003 and references therein). We emphasize that when no AGN heating is considered, the gas cooling rate (top panel) occurring at the very centre of the galaxy roughly decreases in pace with the stellar mass loss ($\dot{M}_* \propto t^{-1.3}$), reaching $\dot{M}_{\rm cool} \approx 1\,\mathrm{M_\odot\,yr^{-1}}$ at $t = 12.7\,\mathrm{Gyr}$, when the simulation ends. Needless to say, this is a much larger cooling rate than allowed by the observations quoted in the Introduction. The rapid initial increase and the peak of $\dot{M}_{\rm cool}$ at $t \sim 1\,\mathrm{Gyr}$ reflect the transient phase during which the ISM is built up by stellar mass loss.

The X-ray luminosity also drops secularly, from $L_{\rm X} \sim 5 \times 10^{42}\,\mathrm{erg\,s^{-1}}$ at $t = 2\,\mathrm{Gyr}$ to $\sim 9 \times 10^{41}\,\mathrm{erg\,s^{-1}}$ at the final time. We refer here to the bolometric X-ray luminosity, calculated within $r \lesssim 200\,\mathrm{kpc}$. The reason for the luminosity drop is the decline of ISM density illustrated in the middle panel of Fig. 1. The slope of the density radial profile does not vary significantly with time and, as expected, is too steep at the centre, a well-known problem of classical cooling-flow models (Sarazin & White 1988; Sarazin & Ashe 1989).

We also note that classical cooling flows in isolated galaxies lack the large cool core typical of cooling-flow clusters or groups (see the spectroscopic-like[3] temperature profile in the third panel). Instead, the temperature increases monotonically towards the centre (except for the very inner region). This can be understood because the steep gravitational potential associated with the peaked de Vaucouleurs' density profile (the dark halo is subdominant within $r_{\rm eff}$) provides enough gravitational heating to the inflowing – thus compressing – gas to balance the radiative losses; needless to say, this process terminates when the gas reaches the centre, where it cools catastrophically.

Ideally, we would compare the profiles with a well-observed elliptical, which is at the same time massive *and* isolated, in the sense of Section 2.2.1. However, most of the known giant ellipticals reside at the centre of groups or clusters and their hot ISM is contaminated by the CGG. NGC 6482 is one of the few massive and X-ray-bright ellipticals with a negative temperature gradient (Khosroshahi et al. 2004) and we show the data of this system in Fig. 1 for comparison. On the other hand, we note that NGC 6482 presents some differences compared with our model. The dark halo is less massive (Khosroshahi et al. 2004; Humphrey et al. 2006) and the object owns a relatively extended X-ray halo with $L_{\rm X} \sim 10^{42}\,\mathrm{erg\,s^{-1}}$, likely contaminated by CGG. Nevertheless, for $r \lesssim r_{\rm eff}$, i.e. the region more relevant to our investigation, the hot gas should be dominated by the internal component only.

3.2 AGN feedback: $\epsilon = 10^{-4}$

We now describe some results for simulations with AGN feedback, progressively increasing the efficiency and focusing on their global properties. We compare them with the cooling-flow model discussed

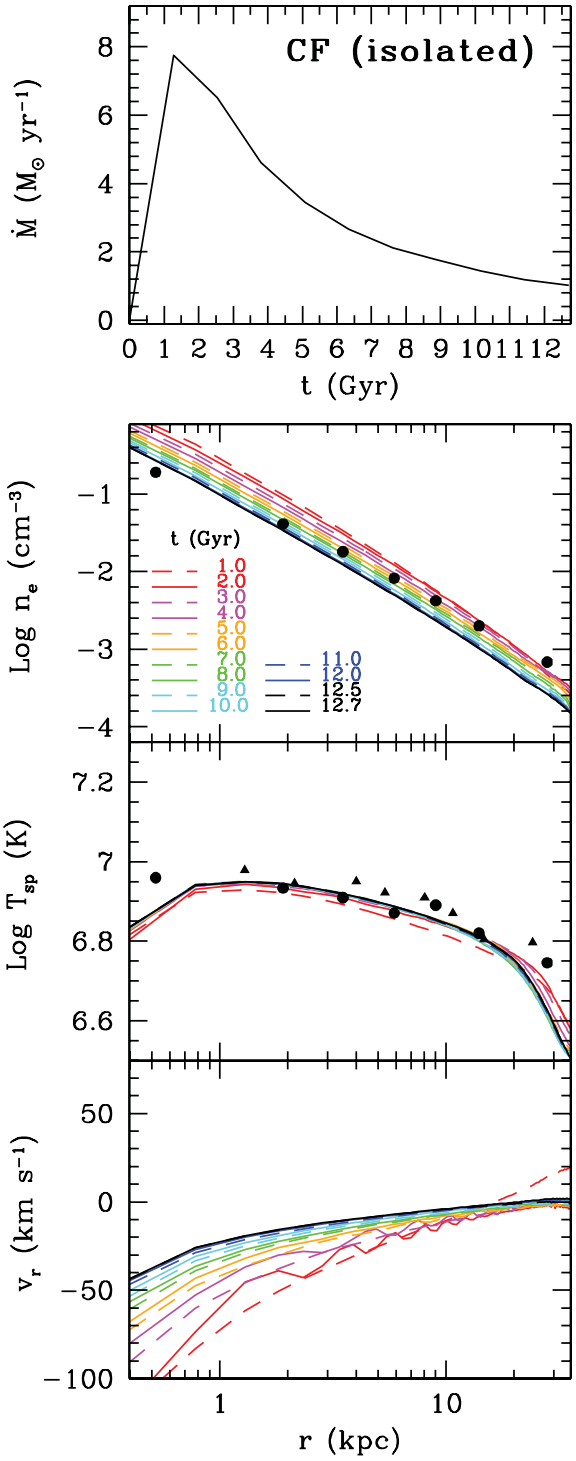

Figure 1. Evolution of the cooling-flow model (no AGN feedback) for an isolated galaxy (iso-CF). From top to bottom: gas cooling rate ($\dot{M}$) as a function of time, radial profiles of electron number density ($n_{\rm e}$), projected spectroscopic-like temperature ($T_{\rm sp}$) and radial velocity ($v_{\rm r}$). Times and colours are indicated in the second panel. Filled points represent observational data for the elliptical galaxy NGC 6482 (circles: Khosroshahi, Jones & Ponman 2004; triangles: Diehl & Statler 2008b). See Section 3.1 for more details.

[3] To adhere more closely to observations, we avoid the idealized emission-weighted temperature; instead we use the prescription by Vikhlinin (2006) to estimate a more realistic projected temperature approximately. The two types of profile nevertheless appear similar in the majority of cases.

above and perform a critical analysis of the observable quantities. The first three rows of Fig. 2 show the gas cooling rate plus the radial profiles of electron number density and (projected) spectroscopic-like temperature for three representative feedback models.

In the first column, top panel, the model with $\epsilon = 10^{-4}$ exhibits a cooling rate significantly reduced with respect to the iso-CF simulation (red/lower versus black/upper line), with an average value of $\sim 0.4\,\mathrm{M_\odot\ yr^{-1}}$ and $\dot{M}(12.7\,\mathrm{Gyr}) \sim 0.2\,\mathrm{M_\odot\ yr^{-1}}$. These numbers are probably still too high compared with available X-ray and UV observations (Bregman et al. 2001, 2005; Xu et al. 2002; Tamura et al. 2003) or star-formation estimates in massive ellipticals (Temi et al. 2009).

The density profile (second panel) oscillates in time, especially in the inner region, but retains reasonable values, as can be noticed through a comparison with typical observations of ellipticals (Humphrey et al. 2006).

The density cycles correspond to the accumulation of gas during periods of less intense AGN activity, e.g. between 6 and 7 Gyr there is no powerful outburst. This leads to an increase of the gas density in the central region, a higher cooling rate and finally a powerful ($\sim 3 \times 10^{44}\,\mathrm{erg\,s^{-1}}$) event that quickly expands the hot gas atmosphere. The density cycles are also reflected in the variation of X-ray luminosity which, in turn, fluctuates in range $10^{41} \lesssim L_\mathrm{X} \lesssim 2 \times 10^{42}\,\mathrm{erg\,s^{-1}}$ (with a mean value of $\sim 10^{42}\,\mathrm{erg\,s^{-1}}$). This variation can in part explain the long-standing problem of scatter in the L_B (or L_K)–L_X diagram (Eskridge, Fabbiano & Kim 1995; Beuing et al. 1999; Ellis & O'Sullivan 2006), along with the occurrence of SNIa winds (Ciotti et al. 1991; David et al. 2006) and the variation of dark halo masses at a given optical luminosity (Mathews et al. 2006).

The temperature profile is a sensitive probe of AGN heating scenarios, yet is often neglected in the comparison with observations. As expected, heating processes originating close to the galactic core often overheat the central ISM, an effect rarely or never observed in real galaxies (Brighenti & Mathews 2002, 2003). The best observed systems (which, unsurprisingly, are the X-ray-brightest) commonly show positive temperature gradients, with the centre hosting the coolest X-ray gas of the system (Humphrey & Buote 2006; Diehl & Statler 2008b). On the other hand, observed galaxies that are isolated or in a less dense environment usually show a moderate negative or flat T gradient.

In the third panel (left column) we show the radial profile of the spectroscopic-like temperature at 12 different times. In this feedback model the ISM is never overheated in the central region and always maintains an acceptable thermal structure (Kim & Fabbiano 2003; Fukazawa et al. 2006; Humphrey et al. 2006; Sansom et al. 2006; Diehl & Statler 2008b; Nagino & Matsushita 2009), i.e. the central negative T gradient is rather shallow and the central temperature remains at or below $\sim 10^7$ K. The lack of a substantial cool core must be ascribed to the absence of the CGG and not to the presence of AGN feedback. Ripples in the temperature profile are caused by weak shock waves generated by the AGN outbursts. These perturbations are somewhat more evident in the pressure profile, not shown here. However, these waves would be largely diluted if the azimuthal average were made in relatively larger radial bins, as in real observations. We did not try here to generate exactly a fully synthetic observation of the simulations (see Heinz, Brüggen & Friedman 2011) and we limit our analysis to spectroscopic-like, projected quantities.

The last three rows of Fig. 2 show the detailed evolution of the mechanical feedback (for the single jet). The total injected energy (E_jet) for this model is 3×10^{59} erg and the typical power (P_jet) is of the order of 3×10^{42}–$10^{43}\,\mathrm{erg\,s^{-1}}$, with velocities ($v_\mathrm{jet}$) around $10^4\,\mathrm{km\,s^{-1}}$.

3.3 AGN feedback: $\epsilon = 10^{-3}$

The previous model, with efficiency $\epsilon = 10^{-4}$, was found to be in satisfactory agreement with several observational constraints. However, the cooling rate, although significantly reduced with respect to the classical iso-CF model, was still too large compared with observational limits. It is thus natural to increase the heating efficiency, essentially a free parameter of any current feedback scheme, to test whether the cooling rate can be further reduced without scrambling the variable profiles.

When $\epsilon = 10^{-3}$ (third column in Fig. 2), the effect of the feedback is excessive: the ISM becomes rarefied in the inner region ($r \lesssim r_\mathrm{eff}$) and simultaneously overheated. Because the $\epsilon = 10^{-3}$ model was unsatisfactory, we stopped this simulation at $t \sim 9.5$ Gyr. It is interesting that the energy released by AGN feedback is lower when the efficiency ϵ is larger (cf. the fourth row of Fig. 2, $E_\mathrm{jet} \gtrsim 10^{59}$ erg). Evidently the more powerful and faster outflows (several $10^{44}\,\mathrm{erg\,s^{-1}}$ and over $5 \times 10^4\,\mathrm{km\,s^{-1}}$) of the iso-1em3 model are able to stop the cooling flow for a relatively long time. The interval between AGN outbursts is in fact $\sim 6 \times 10^7$–10^8 yr, while for $\epsilon = 10^{-4}$ the AGN activates at least one order of magnitude more frequently, with the net result of injecting less energy over the galaxy lifetime. This confirms the same trend found for galaxy clusters (G11a) and illustrates that the complexity of the problem makes reasoning based on the energetic budget alone rather inaccurate.

The lower gas density implies a generally lower X-ray luminosity, with mean $\sim 5 \times 10^{41}\,\mathrm{erg\,s^{-1}}$. With efficiencies $\epsilon > 10^{-3}$ (models not shown), the simulated profiles depart strongly from those of real ellipticals (like NGC 6482) and the X-ray luminosity drops to undetectable values. We note here that low-L_X early-type galaxies usually show the presence of some ISM in the central region, which has a relatively low temperature (see for example NGC 4697: Sarazin, Irwin & Bregman 2001; NGC 1291: Irwin, Sarazin & Bregman 2002; NGC 3379: Trinchieri et al. 2008). Thus, their low X-ray luminosity may not be associated with strong AGN feedback generating a galactic wind.

3.4 AGN feedback: $\epsilon = 3.3 \times 10^{-4}$

Finally, we have calculated a model with intermediate efficiency, $\epsilon = 3.3 \times 10^{-4}$, which will serve as the best model in the following discussion. As displayed in the middle column of Fig. 2, the cooling rate is now below the limits placed by current observations ($\lesssim 0.1\,\mathrm{M_\odot\ yr^{-1}}$), apart from a narrow, transient peak at $t \sim 4$ Gyr. The density and temperature profiles vary in time slightly more than in model iso-1em4, but remain consistent with observations (cf. NGC 6482 data points). The spatial oscillations in the (projected) temperature profiles, with maximum amplitude ~ 20 per cent, are compatible with those shown in deep *Chandra* observations (see for example fig. 10 in Randall et al. 2011).

The final injected energy is 10^{59} erg (fourth panel). Typical outburst powers are in the range several 10^{42}–few $10^{44}\,\mathrm{erg\,s^{-1}}$ (fifth panel), while the velocity of the outflows (bottom panel) varies in the range[4] 10^3–$10^5\,\mathrm{km\,s^{-1}}$, in good agreement with nuclear outflow

[4] The relativistic factor $\gamma \sim 1.06$ is still low enough to use classic hydrodynamics safely.

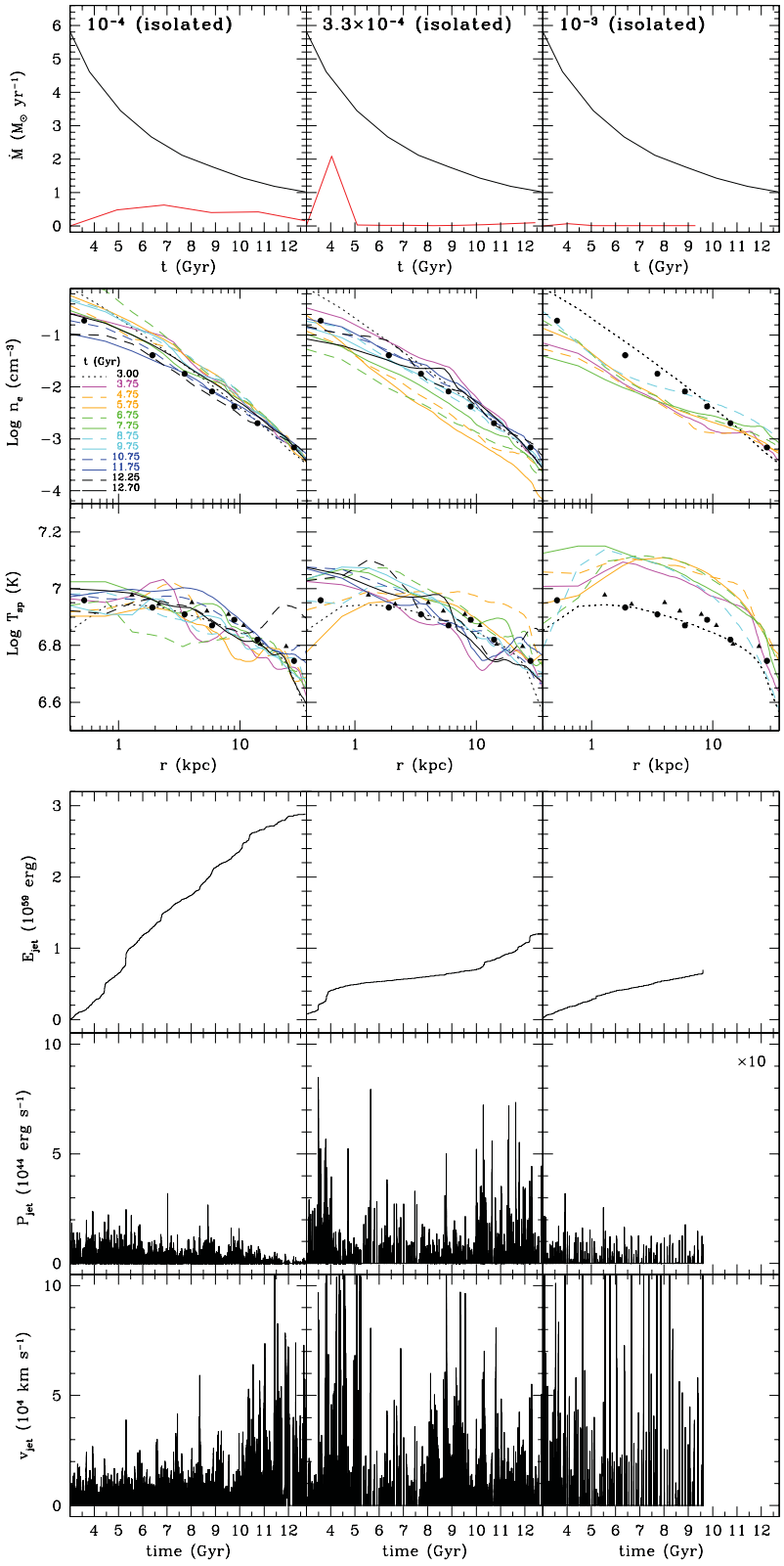

Figure 2. Evolution of an isolated galaxy with AGN feedback and increasing mechanical efficiency (from left to right column): $\epsilon = 10^{-4}$, 3.3×10^{-4} and 10^{-3}. First three rows: gas cooling rate versus time (red/lower: AGN feedback; black/upper: pure cooling flow), radial profiles of electron number density and spectroscopic-like temperature (at 12 different times). Last three rows: injected mechanical energy, instantaneous power and velocity of the AGN feedback (for the single outflow) as a function of time.

and feedback observations (see Introduction). The power values correspond to instantaneous accretion rates $\dot{M}_{\rm acc} = P_{\rm jet}/(\epsilon c^2) \sim 0.1$–$10\,{\rm M}_\odot\,{\rm yr}^{-1}$. The frequency of the AGN activation is usually in the range 2×10^{-2}–$5 \times 10^{-2}\,{\rm Myr}^{-1}$, albeit it varies significantly during the flow evolution. We point out that the details of the AGN duty cycle depend on the ability to resolve the condensing cold clouds in space and time and thus on the numerical resolution adopted.[5] Nevertheless, the cold feedback self-regulation is robust enough that the cooling-flow problem is solved irrespective of the duty-cycle details.

We consider iso-3em4 the best model because the cooling rate is in good agreement with known constraints for many Gyr and the variable profiles always resemble those of real galaxies. Thus, this model (and to a lesser extent iso-1em4) passes the first checkpoint, a necessary condition for a viable heating mechanism. In order to test the robustness of the model further, in the next section we analyse the detailed galaxy appearance in the X-ray band. Finally, we note that the value of the ϵ parameter should not be taken as the exact physical value, given the uncertainties in the simulated accretion rate (Section 2.1.1).

3.4.1 X-ray features

In this section we investigate the most significant X-ray features naturally generated by the AGN heating process, like shocks and buoyant cavities. A direct comparison with a specific real system is not possible because our models are intended to be general and not tailored to an individual object. Moreover, cavities, shocks and perturbations are intermittently created, continually changing the ISM appearance. The main aim of the analysis is to show that the proposed feedback mechanism leads to ISM perturbations similar to those observed in galaxies and groups. A feedback scenario not satisfying basic requirements, such as the formation of cavities or weak shocks, must be rejected.

We discuss below several X-ray snapshots, taken at different times, of the best model iso-3em4. In Fig. 3 (panel a in the top row) we show the X-ray surface-brightness map of the central region after 0.75 Gyr of feedback evolution. An outburst with energy 2.85×10^{56} erg occurred 8×10^6 yr before the time of the snapshot. The outflow, ejected with velocity $v_{\rm jet} \sim 5400\,{\rm km\,s}^{-1}$, generated a weak shock, now at a distance $\sim$6 kpc from the centre, with a Mach number $M \approx 1.2$ (calculated from $T_{\rm sp}$, which jumps from $\sim$0.5 keV in the pre-shock region to $\sim$0.6 keV in the post-shock ISM). The outflow generated a small X-ray cavity centred at $z = 4.5$ kpc of ellipsoidal (prolate) shape with semiaxes 1.5 and 1 kpc. The X-ray surface-brightness depression within the cavity is about 20 per cent, a typical value for observed cavities. Relatively colder rims surround the cavity, although the $T_{\rm sp}$ difference between the rims and the nearby gas is only $\sim$10 per cent (Fig. 3b). We note that the ISM adjacent to the rims has been slightly heated by the weak shock. In the spectroscopic-like temperature map very weak waves are also visible (but probably not detectable with current X-ray telescopes), separated by $\Delta r_{\rm waves} \sim 6$ kpc, corresponding to a period of $t_{\rm waves} = \Delta r_{\rm waves}/c_{\rm s} \sim 1.6 \times 10^7$ yr, roughly the typical time between significant AGN outbursts at this epoch ($t = 3.75$ Gyr). We stress that these X-ray features are faint and the ISM looks quite relaxed at this time.

The situation after 0.5 Gyr ($t = 4.25$ Gyr; Fig. 3c and d) is different. At this epoch the AGN is more active and perturbs the ISM in a remarkable way. The X-ray arms and cavity have been generated by four series of AGN outbursts of moderate power (a few $10^{42}\,{\rm erg\,s}^{-1}$) that occurred during the previous 10 Myr. The energy injected during this time interval is $\sim 1.4 \times 10^{57}$ erg. Fig. 3(c) shows that the X-ray surface brightness map is rich in features, with two symmetric bright arms $\sim$15 kpc long. This structure is similar to that observed in NGC 4636, a massive elliptical galaxy in the outskirts of the Virgo cluster (Jones et al. 2002; Baldi et al. 2009). Thus, it might be possible that the ISM of NGC 4636 has been shaped by multiple, moderate AGN outflows. It is in fact difficult to reproduce all the observed features of NGC 4636 with a single AGN outburst (Ballone & Brighenti, in preparation).

In the spectroscopic-like temperature map shown in Fig. 3(d), the X-ray-bright arms are slightly hotter than the local ISM. The temperature jump is about 30 per cent (from 0.67 to 0.89 keV) corresponding to a shock Mach number of $\sim$1.3.

The galaxy alternates periods of quiescence, typically lasting 50–100 Myr, with moments during which the AGN is more active and consequently the ISM more disturbed. Other interesting features appear during the evolution. At $t = 5.75$ Gyr a cold front is visible in both the brightness and temperature maps, at $\sim$2 kpc from the centre (Fig. 3e and f). The front has not been caused by galaxy-sloshing in our simulations but by the encounter between gas that is falling back towards the centre after an outflow and the gas currently located in the central region.

At $t = 6.25$ Gyr (Fig. 3g) the brightness map shows a weak cavity about 3 kpc in radius, surrounded by a $\sim$10 kpc shock with Mach number $\sim$1.3 (Fig. 3h). This situation is similar to that at $t = 3.75$ Gyr, described in Fig. 3(a). This demonstrates that the ISM evolves cyclically, with recurrent cavities generated by the outflows and weak shocks, just as indicated by observations.

Although not a common circumstance, a series of shocks are visible at the same time. This occurrence is shown in Fig. 3(i) ($t = 11.75$ Gyr), where two ellipsoidal shocks are depicted (Mach $\sim$1.4–1.5). The shocks intersect the y-axis at $\sim$4 and $\sim$8 kpc and are clearly visible in both surface-brightness and temperature maps (Fig. 3j).

This brief description of the ISM appearance in the X-ray band is intended to illustrate the richness of structures generated by AGN outflows. Although in the present study we do not attempt a detailed comparison with real objects, it is important to realize the strong similarity of simulated features, like X-ray cavities, filaments and shocks, to the structures seen in deep X-ray observations of ellipticals and groups (Biller et al. 2004; Machacek et al. 2006, 2011; Baldi et al. 2009; Gastaldello et al. 2009; O'Sullivan et al. 2011b; Randall et al. 2011). This fact, together with the analysis in the previous section, indicates that AGN outflows are indeed a very robust feedback mechanism, capable of strongly inhibiting gas cooling, keeping reasonable density and temperature profiles and giving rise to the wealth of asymmetric structures in the ISM seen in high-resolution deep X-ray observations.

4 RESULTS: CIRCUMGALACTIC GAS

As previously mentioned, most massive, X-ray-bright ellipticals host a very extended hot ISM that cannot be explained via internal processes alone (Brighenti & Mathews 1998, 1999). These galaxies are at the centre of large dark matter haloes (Mathews et al. 2006) and the ISM is likely composed of gas shed by the stellar population

[5] The duty cycle is thus linked to the thermal instability time-scale, roughly the local cooling time, and also to the free-fall time (see Gaspari et al. 2012 for complete multiphase gas simulations with self-regulated AGN jet feedback).

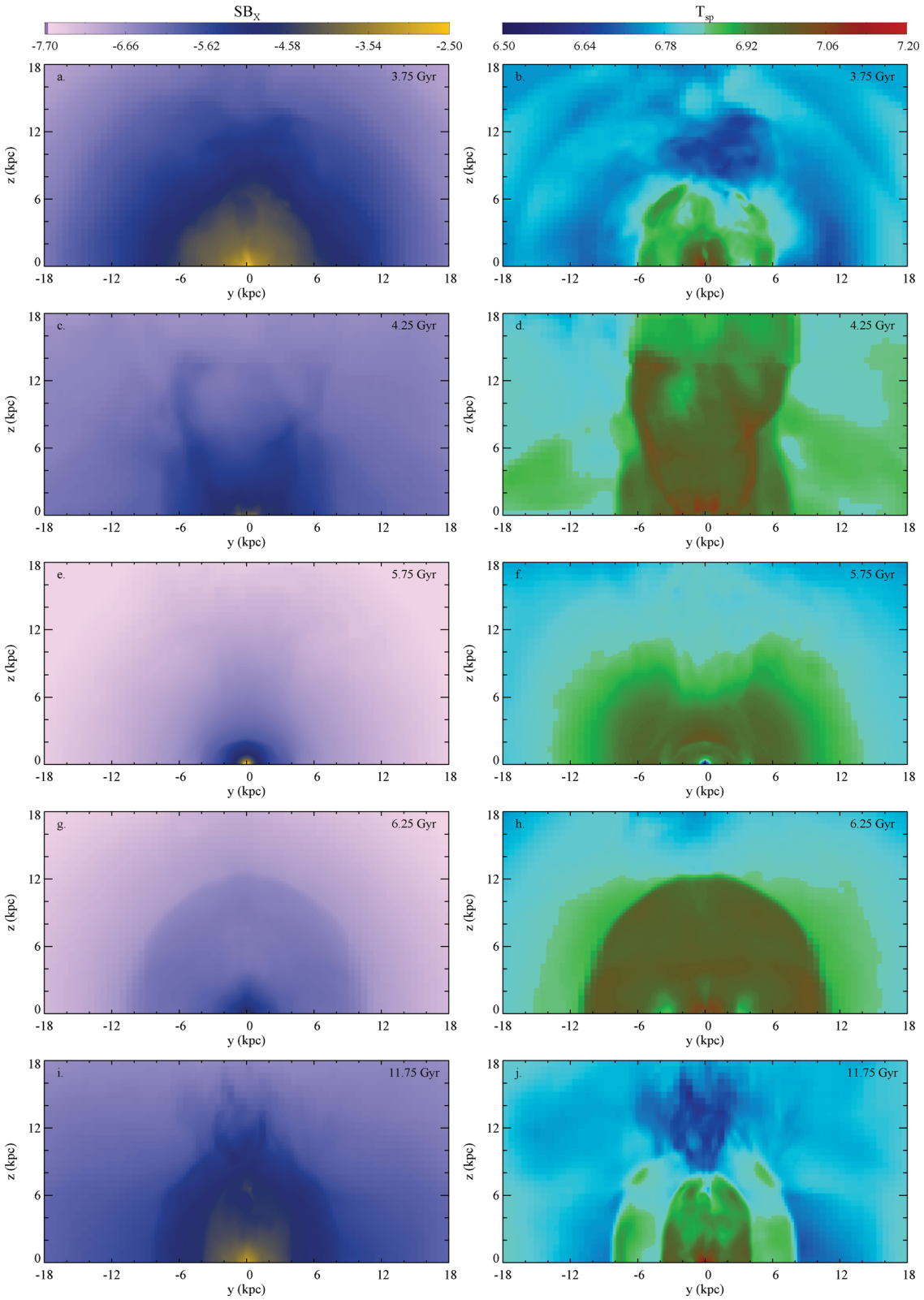

Figure 3. Maps of X-ray surface brightness (left column) and projected spectroscopic-like temperature (right column) for model iso-3em4 at five different times (from top to bottom row): 3.75, 4.25, 5.75, 6.25 and 11.75 Gyr. See Section 3.4.1.

plus circumgalactic gas linked to cosmological evolution. It is thus important to test whether mechanical AGN outflows are successful for this class of objects, which includes many famous X-ray targets such as NGC 4636, NGC 4472, NGC 5044 and NGC 4649.

Interestingly, in these cool-core objects the evidence for AGN heating seems stronger, as revealed by the presence of X-ray cavities and other ISM perturbations (Biller et al. 2004; Diehl & Statler 2008a; Baldi et al. 2009; Gastaldello et al. 2009; Dong, Rasmussen & Mulchaey 2010; Dunn et al. 2010b; Randall et al. 2011; O'Sullivan et al. 2011b). It might be a selection effect, but it is ironic (and instructive) to note that, just where we know the AGN is injecting energy, the ISM close to the feedback engine is cooler than everywhere else.

4.1 AGN feedback: $\epsilon = 8 \times 10^{-4}$

In this section we present only the best feedback model for a CGG elliptical (efficiency $\epsilon = 8 \times 10^{-4}$), able properly to solve the cooling-flow problem. It is interesting that the same feedback method now requires a larger efficiency to be acceptable, in line with the results of G11b, which indicate that in more massive systems the feedback should act more efficiently.

As in the case of an isolated galaxy, we have run a classic cooling-flow model (no AGN heating), which serves as a reference calculation to gauge the effects of the feedback. We do not show the evolution of the pure CF profiles here (cgg-CF). The results are almost identical to those presented in G11b, although the numerical resolution there was about two times coarser ($\Delta x \approx 500$ pc) compared with the present model. The gas cooling rate, also indistinguishable from that in G11b, is shown in Fig. 4 (black line in the top left panel). As suggested by the resulting bolometric $L_{\rm X} \sim 3 \times 10^{43}$ erg s^{-1}, the cooling rate stays around $\sim$25 M$_\odot$ yr^{-1}, once more revealing the cooling-flow problem at the galactic/group scale.

The AGN feedback model with $\epsilon = 8 \times 10^{-4}$ (cgg-8em4) is fully presented in Fig. 4. The cooling rate (red/lower line, first panel) has been quenched to $\sim$1 M$_\odot$ yr^{-1} at the current epoch, implying a satisfactory 20-fold cooling suppression, broadly consistent with *X-ray Multi-Mirror Mission* (*XMM*) Reflection Grating Spectrometer (RGS) observations (Tamura et al. 2003).

The spectroscopic-like temperature and density radial profiles are in excellent agreement with those observed for NGC 5044 (left column: middle and bottom panel). Remarkably, the cooling reduction did not come at the expense of the cool core: the temperature still decreases towards the galactic centre, a fundamental quality of anisotropic mechanical feedback.

The total mechanical energy released by the AGN is $E_{\rm jet} \sim 9 \times 10^{60}$ erg (first panel in second column), which in principle would

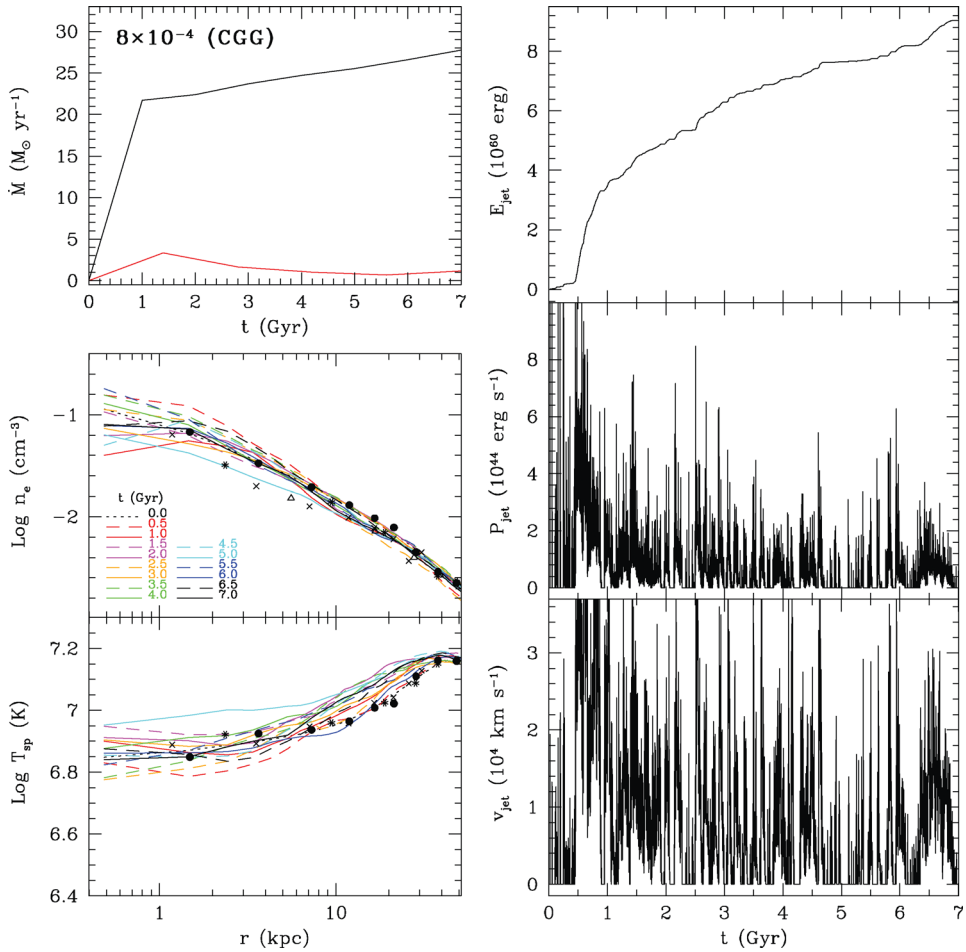

Figure 4. Evolution of an elliptical galaxy with circumgalactic gas and mechanical feedback efficiency $\epsilon = 8 \times 10^{-4}$. Left column, from top to bottom: cooling rate as a function of time (red: AGN feedback; black: pure cooling flow); electron number density and spectroscopic-like temperature at several times. The points in the last two panels represent observational data of the bright elliptical NGC 5044 (David et al. 1994; Buote et al. 2003). Right column: injected mechanical energy, (single) outflow power and velocity as a function of time.

correspond to a total mass accreted on to the black hole of $\sim 6 \times 10^9\,\mathrm{M}_\odot$, given the assumed efficiency. This accreted mass may appear substantial, but we stress again that the simulated accretion rate is quite uncertain (supermassive black holes (SMBHs) can nevertheless reach masses of a few $10^{10}\,\mathrm{M}_\odot$). We note that the BH growth could in principle be reduced by assuming that a fraction of the cooling gas does not accrete on to the BH and is ejected with the AGN outflow; increasing the efficiency would produce the same feedback power (but adding another parameter to the scheme would not provide any further physical insight).

The most relevant astrophysical result here is that self-regulated massive outflows are indeed capable of solving the cooling-flow problem on kpc or larger scales, although the fully consistent picture – explaining the details of the BH accretion process and the formation of the outflows – needs to be clarified in future via high-resolution investigations.

The time record of the outflow power and velocity is shown in the right column of Fig. 4. Powers of the order of a few $10^{44}\,\mathrm{erg\,s^{-1}}$ and velocities of several $10^4\,\mathrm{km\,s^{-1}}$ are again typical for the stronger events.

We conclude that massive outflows, activated when gas cooling occurs, are able to regulate the thermal evolution of the ISM, suppressing the cooling rate by a factor of 20 or more and keeping the cool-core aspect of massive, X-ray-bright ellipticals. We now test the model via other key observational constraints.

4.1.1 X-ray features

The variety in X-ray features induced by AGN outflows in an isolated galaxy (Section 3.4.1), such as buoyant bubbles and shocks, is also widely present in the CGG simulation. For cgg-8em4 we find that the AGN activity is more frequent and powerful compared with an isolated galaxy (cf. Figs 2 and 4). Nevertheless, the X-ray appearance of the two models is remarkably similar.

In the first row of Fig. 5, we show the X-ray surface brightness and spectroscopic-like projected temperature at $t = 0.5\,\mathrm{Gyr}$ (Fig. 5a and b). We focus our attention on the inner $20 \times 10\,\mathrm{kpc}^2$ of the maps, where the observations could return better details. The outflow has carved a long cavity (or channel) $\sim$10 kpc long and $\sim$2 kpc wide. The brightness depression is about a factor of 2, which should make this feature detectable in deep, high-resolution images. For $z \lesssim 4\,\mathrm{kpc}$ the cavity is surrounded by sharp bright rims (or filaments), which are reminiscent of the southern open cavity in NGC 5044 (Buote et al. 2003; David et al. 2009; Gastaldello et al. 2009). The cavity is slightly hotter (by $\sim$10 per cent, see $T_{\rm sp}$) than the nearby gas. At $z \gtrsim 6\,\mathrm{kpc}$, broad regions ($\Delta y \sim 3\,\mathrm{kpc}$) of enhanced surface brightness, confining the X-ray feature, are present. This channel is typically fragmented by AGN turbulence or strong recurrent outbursts, and would also be destroyed by the bulk motion ('weather') induced by the cosmological accretion of matter on to the system. On the $z = 0$ plane, close to the centre, the inflowing gas forms a dense torus that is punched, but not cleared away, by the outflows. This feature could, however, be numerically amplified by the forced planar symmetry ($z = 0$ plane), where reflection boundary conditions are implemented.

At $t = 1\,\mathrm{Gyr}$ (Fig. 5c), the $SB_{\rm X}$ map shows a region of enhanced emission, several kpc in size, close to the centre of the galaxy ($0 \lesssim y \lesssim 5\,\mathrm{kpc}$). This is caused by relatively dense and cold gas, some of which is actually cooling to low temperatures ($T \lesssim 10^5\,\mathrm{K}$) and has dropped out from the flow (Fig. 6a). This is a very interesting phenomenon, because the off-centre cooling might explain the widespread presence of cold ($T \sim 10^4\,\mathrm{K}$) gas in large ellipticals with conspicuous hot gas (see references quoted in the Introduction). Despite being linearly stable against thermal instability (e.g. Balbus 1988; Balbus & Soker 1989; Loewenstein 1989; Malagoli, Rosner & Fryxell 1990), the non-conducting hot gas may well cool if the amplitude of the perturbations is sufficiently large (Reale et al. 1991; Yoshida, Habe & Hattori 1991; McCourt et al. 2012; Sharma et al. 2012). High-resolution X-ray maps indeed show a wealth of irregularities in the hot gas, which certainly imply large perturbations in the gas density. Localized gas density enhancements are naturally generated in regions of converging flows, resulting in local cooling times much lower than the free-fall times. This allows the gas to reach very low temperatures, $T \approx 5 \times 10^4\,\mathrm{K}$, when it is removed from the grid (see also Brighenti & Mathews 2002). The process of multiphase gas formation (in cluster cores heated by AGN jets) has been investigated in depth by our recent work, Gaspari et al. (2012), showing that the non-linear perturbations associated with the AGN jet feedback commonly induce the condensation of hot gas into a filamentary extended cold phase (as also indicated by Fig. 6, left panels).

Cooling gas at large distance from the galactic centre is also seen at $t = 2\,\mathrm{Gyr}$ (Fig. 5, panel e) in an enhanced $SB_{\rm X}$ region defined by $z \lesssim 1\,\mathrm{kpc}$ and $R \lesssim 7\,\mathrm{kpc}$. Several cavities surrounded by relatively cold, bright rims rise buoyantly on various scales (Fig. 5, panel f), while very weak shocks vanish rapidly as sound waves at large radii. The cold rims are metal-rich, as expected, being formed by gas originally at the centre of the galaxy. In the present model, in fact, we followed the chemical enrichment of the hot gas halo, with emphasis on the evolution of the iron expelled by SNIa. The map of the (emission-weighted) iron abundance is shown in Fig. 6(b). The AGN outflows generate asymmetries in the Fe distribution: the relatively metal-rich gas originally in the centre is uplifted along the direction of the outflow and cavities. This results in regions of enhanced iron abundance (by 20–30 per cent) which trace the dynamics of the recent outflows. Besides this global behaviour, kpc-sized inhomogeneities are also evident in the abundance map. The ability of mechanical feedback to dredge up cold, metal-rich gas from the centre of the system could in principle be used to discriminate between outflows or thermal feedback mode.

At $t = 4\,\mathrm{Gyr}$ (Fig. 5, panels g and h) a complex structure is visible in the X-ray surface-brightness image, mainly due to the generation of multiple cavities and bright filaments. As usual, brightness contrasts are accompanied by temperature and metallicity variations, here of the order of 10 per cent. These images show that recurrent AGN outflows naturally generate and drive turbulence in the core, with typical velocities of a few hundred $\mathrm{km\,s^{-1}}$ (see Section 5.1.1). The chaotic turbulent environment naturally produces complex irregular features, at the same time increasing the level of thermalization in the central region via jet fragmentation.

At $t = 6.5\,\mathrm{Gyr}$ (Fig. 5, panels i and j), almost at the end of the simulation, we observe irregular regions of high surface brightness in the central few kpc, where the gas cools to very low temperatures producing diffuse Hα emission. Fig. 6(c) provides the total dropped cold mass (integrated in time), again indicating that the cold phase condenses out of the hot flow not only at the very centre but in an extended region of radius 7–15 kpc. The drop-out term in the equations used prevents a detailed analysis of the thermal instability; we refer the reader to Gaspari et al. (2012), where fully multiphase simulations are presented. Quantifying the exact amount of gas cooling far from the centre is a difficult problem (due to numerical diffusion and resolution). Nevertheless, the result is qualitatively robust: off-centre cooling exists, as indicated by observations (McDonald,

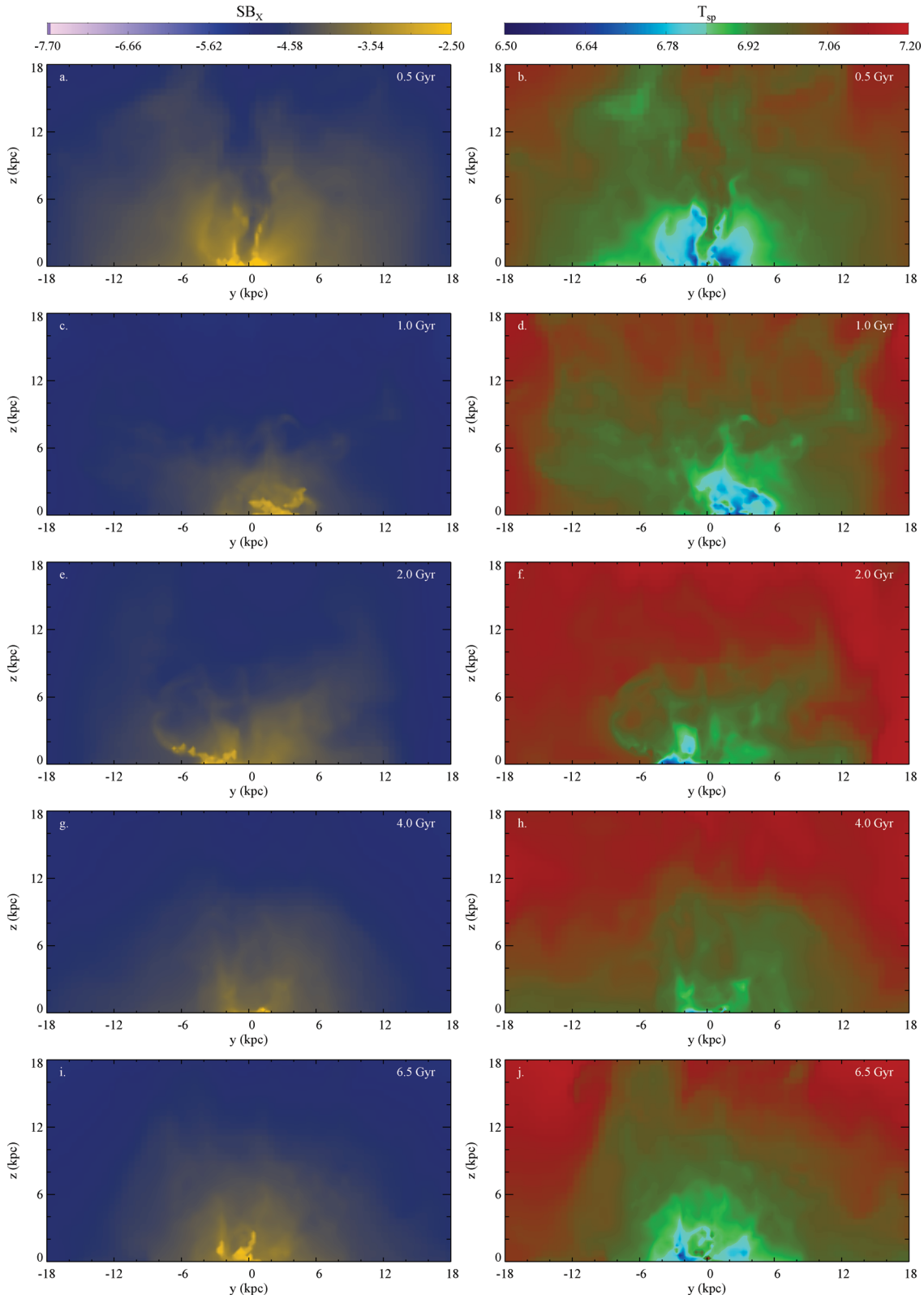

Figure 5. Maps of X-ray surface brightness (left) and projected spectroscopic-like temperature (right) for the best model with circumgalactic gas (cgg-8em4), at five different times (from top to bottom): 0.5, 1.0, 2.0, 4.0 and 6.5 Gyr. See Section 4.1.1. For time 2.5 Gyr we present both the *x*-axis (top) and *z*-axis (bottom) projections of the SB_X and T_{sp} map.

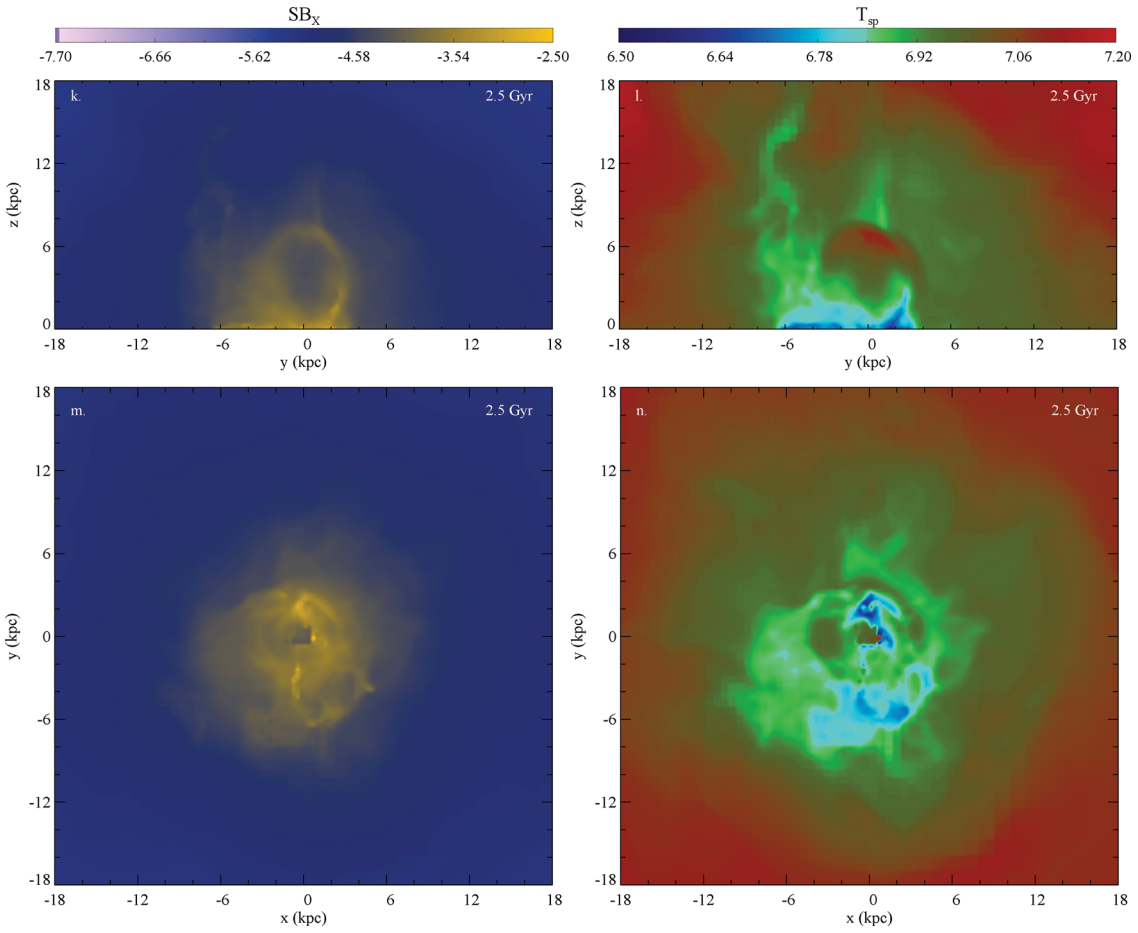

Figure 5 – *continued*

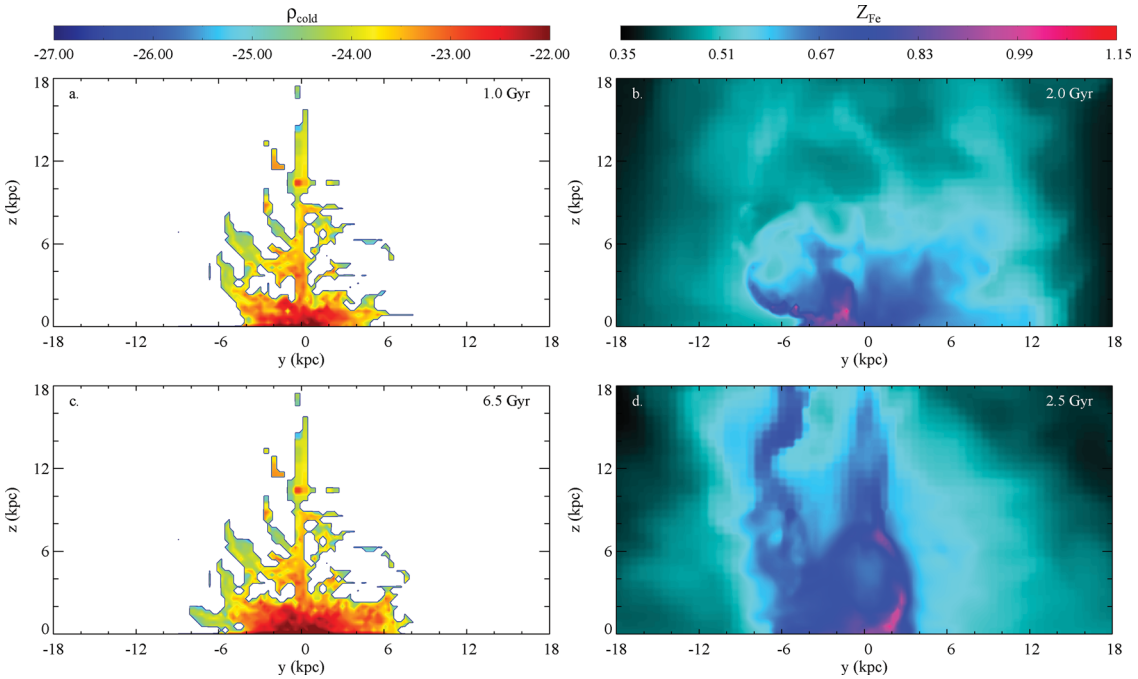

Figure 6. Maps of total dropped cold gas ($T \leq 2 \times 10^4$ K; left) and emission-weighted iron abundance (right), both projected along the x-axis, for model cgg-8em4 at different times; see Section 4.1.1.

Veilleux & Mushotzky 2011) and it can be triggered by the AGN feedback process.

We conclude the snapshot analysis for the CGG model by showing a textbook example of an X-ray cavity confined by bright rims (Fig. 5, panels k and l). The largest brightness contrast between the X-ray hole and the rims is about a factor of 2. From the spectroscopic-like temperature map, we see that the lower part of the rims ($z \lesssim 3$ kpc) is colder in projection than the nearby ISM, while the upper part is slightly hotter because of shock heating. Again the rims, since they originate from the central gas, are slightly more metal-rich than the ISM at the same radius, by 15–25 per cent in iron abundance (Fig. 6d). For this time, we also show the projection along the z-direction (Fig. 5m and n). Several structures and cavities are visible, together with X-ray-bright filaments. In this projection, $T_{\rm sp}$ is characterized by an arc-shaped region about $\sim$20 per cent colder than the neighbouring gas. This comparison between two different projections warns us how complicated the interpretation of real data is, especially when the inclination of the outflow, with respect to the plane of the sky, is uncertain.

The generation of buoyant bubbles, together with all the previous consistent observational features (extended multiphase gas, metals asymmetries, turbulence, weak shocks), strengthens the key role of mechanical AGN outflows in regulating the thermal and dynamical evolution of elliptical galaxies, with or without circumgalactic gas.

5 CONCLUDING REMARKS

5.1 AGN feedback in elliptical galaxies

In the previous sections we have investigated the effect of AGN feedback on the evolution of the ISM in massive elliptical galaxies. In designing 3D hydrodynamic simulations, we have been guided by several ideas.

(i) The AGN feedback in low-redshift elliptical galaxies acts mainly through a (radiatively inefficient) mechanical and directional process, in the form of jets or winds.

(ii) These outflows interact with the ISM and heat the medium on scales of several kpc, as indicated by X-ray observations of cavities and shocks.

(iii) The AGN reacts to gas cooling: cold gas condenses out of the hot phase in the central region and is assumed to be accreted on to the black hole in a few dynamical times, triggering AGN feedback. The uncertainties in the the real accretion rates force us to adopt as simple a parametrization as possible (the only governing parameter being the mechanical efficiency ϵ). Given the uncertainties mentioned in Section 2.1.1, we are not in a position to investigate important issues such as exact BH growth or the details of the AGN duty cycle.

(iv) The feedback mechanism must work for objects of any scale, from isolated galaxies to massive galaxy clusters.

(v) The calculated evolution of the hot gas must be checked against many available observational constraints, for a long time span (several Gyr).

In G11a,b we have shown that AGN outflows are able to solve the cooling-flow problem for both massive clusters and groups, for more than 7 Gyr. We are left now to demonstrate that these mechanical massive outflows, self-regulated by cold accretion, also represent the dominant feedback mechanism on galactic scales.

In Section 3 we have discussed several models for an isolated elliptical, while the more astrophysically relevant case, i.e. a galaxy with circumgalactic gas, is tackled in Section 4. The two key tests that the models must pass are agreement with the low cooling rates allowed by observations (*no overcooling*) and a moderate gas temperature in the central region of galaxies (*no overheating*). The former sets a lower limit on the feedback mechanical efficiency, the latter provides an upper bound.

In Figs 2 and 4 we showed that, assuming an efficiency $\epsilon \gtrsim 3 \times 10^{-4}$ ($\epsilon \gtrsim 8 \times 10^{-4}$) for the isolated (CGG) model, the cooling rate drops to values close to the observational limits reported in the Introduction. The previous values for the mechanical efficiency are lower than those working for clusters (G11a) and similar to those quoted in Ciotti & Ostriker (2007), although for a different feedback scheme. Because our estimated accretion rate on to the BH is likely an upper limit, a firm result of our calculations is that the mechanical efficiency must be $\epsilon \gtrsim$ a few $\times 10^{-4}$ in order to prevent significant gas cooling in massive elliptical galaxies. It is more difficult to place an upper bound on the efficiency. We have shown in Section 3 that when $\epsilon \gtrsim 10^{-3}$ the AGN feedback is too intense and the ISM in the central region is overheated. However, larger mechanical efficiencies would be allowed if the accretion rate were grossly overestimated in our simulations.

While the exact details of feedback engine (such as the duty cycle) are uncertain and must be investigated by high-resolution, specialized simulations, the astrophysically most relevant and solid result of this work is that AGN outflows can also *solve the cooling-flow problem* in elliptical galaxies, drastically quenching the cooling rates and properly maintaining a quasi-thermal equilibrium in the core. This is a remarkable result, given the difficulties encountered with the commonly used thermal feedback (regardless of its origin, i.e. artificially inflated bubbles or radiative heating).

They also agree with a number of other key and independent observational constraints, as illustrated in Sections 3 and 4. A crucial requirement for an AGN feedback scenario is the ability to produce (weak) shocks, X-ray cavities and abundance inhomogeneities, common features shown in deep X-ray observations (see references in the Introduction). These properties point towards a feedback mechanism able to distribute energy and momentum in a directional way, on scales of several kpc. Observationally, these ISM perturbations are best studied in X-ray-bright objects, often giant ellipticals with CGG or groups. About 25–50 per cent of galaxies/groups observed at high resolution show evidence of cavities (McNamara & Nulsen 2007; Dong et al. 2010), a number that is likely underestimated. In galaxy clusters the detection fraction rises to $\gtrsim 2/3$ (Dunn & Fabian 2006). Moreover, cavities are more likely present in cool-core systems (Dong et al. 2010), implying that the feedback action must preserve positive temperature gradients. Elliptical weak shocks are also commonly found (Gitti et al. 2012) surrounding stable buoyant cavities, a natural by-product of jets and outflows (G11a,b).

In Sections 3.4.1 and 4.1.1 we have illustrated the wealth of observable features created by the (anisotropic) mechanical feedback scenario. Deep X-ray observations of galaxies (e.g. NGC 4472: Biller et al. 2004; NGC 4374: Finoguenov et al. 2008; NGC 4636: Baldi et al. 2009) and groups (e.g. NGC 5044: David et al. 2009; HCG 62: Gitti et al. 2010; NGC 5813: Randall et al. 2011; NGC 5836L Machacek et al. 2011) reveal a wealth of features certainly linked to the AGN feedback outbursts. In particular, the two typical fingerprints naturally left by collimated AGN outflows, i.e. X-ray cavities surrounded by a weak shock, are seen in many snapshots of Figs 3 and 5, often also resembling observations from a quantitative point of view (e.g. elliptical cocoons, Mach number, bubble size and temperature). It is impossible to make a 1:1 comparison with real objects, catching the exact evolutionary moment, with the same in-

stantaneous feedback values. Unfortunately, we are not in a position to calculate the time fraction during which the simulated cavities or shocks are visible; this would in fact require an analysis of the flow very finely spaced in time, the subject of a future investigation.

Typically, the cavities inflated by the outflows have size of few kpc and are surrounded by bright rims (e.g. Fig. 3: $t = 3.75$, 4.25 and 11.75 Gyr; Fig. 5: $t = 0.5$, 2.0, 2.5 and 4.0 Gyr). The rims are often slightly cooler and metal-richer compared to the nearby gas, although there are few exceptions. It is worth mentioning that dedicated simulations tailored for NGC 4636 indicate that it is possible to explain most of the properties of the cavities detected in NGC 4636, assuming the feedback proposed in this work (Ballone & Brighenti, in preparation).

In the case of a galaxy with CGG (similar to a group environment), the frequent AGN activity causes the common presence of a low-density channel along the z-direction carved by the outflows, $\lesssim$1kpc wide and several kpc long. This feature is very difficult to detect in the surface brightness map. In Fig. 5 we see that only at the beginning of the calculation, at $t = 0.5$ kpc, is the tunnel visible, with a brightness contrast of ∼2–3 (rapidly decreasing beyond $z =$ 5 kpc). Most of the time, the thin channel is wiped out in the brightness image by projection effects (see also G11b). Occasionally, the tunnel may resemble an X-ray cavity (Fig. 5, $t = 2$ Gyr). A dedicated analysis through very deep X-ray observations in the core of the galaxy may detect this feature, or at least set constraints on its presence (see, for instance, the $SB_{\rm X}$ contours in the inner 3 kpc of NGC 5813: Randall et al. 2011). The channel is nevertheless a transient feature, easily fragmented and destroyed by AGN turbulence (and by the ICM 'weather' generated by cosmological accretion, not considered here), a key element for the proper deposition and thermalization of mechanical energy in the core (Section 5.1.1).

The proposed AGN feedback mechanism has another impact on the gas cooling process, beside significantly lowering the total rate. It promotes spatially distributed cooling (via thermal instabilities) over an extended region of size ∼15 kpc centred on the BH. The left column of Fig. 6 shows the density map of total cold gas that has cooled and dropped out of the flow, highlighting both the extended and concentrated toroidal distribution of cooler gas (consistent with Gaspari et al. 2012). Our code does not follow the dynamics of the cooling gas, but it is plausible that some of the cooled gas accretes on to the BH and some is instead used to form new stars and the emission-line nebulae commonly observed in elliptical galaxies (see the Introduction). At the moment of cooling, the gas has a chaotic motion, with typical velocities of 100–200 km s^{-1} concordant with Hα spectroscopic studies (Caon et al. 2000).

Mechanical feedback is also able to reproduce the anisotropic distribution of metals commonly observed in AGN-heated cores (Rasmussen & Ponman 2009; David et al. 2011; Kirkpatrick et al. 2011; O'Sullivan et al. 2011a). Powerful mechanical jets can indeed uplift the metals processed by SNIa and stellar winds in the nuclear region up to ∼10 kpc (with a peak metallicity of $Z_{\rm Fe} \lesssim 1\,{\rm Z}_\odot$: Mathews & Brighenti 2003). In the more quiescent phases, AGN turbulence tends instead to stir and diffuse the metals, restoring a homogeneous distribution (Fig. 6, right panels).

5.1.1 AGN turbulence

Another test the feedback model must pass, although less stringent than those previously discussed, is the generation of turbulence (or bulk motion) in the ISM, especially in the central region. Deep X-ray observations start to provide reliable estimates of the turbulent pressure (Werner et al. 2009; Sanders, Fabian & Smith 2011; de Plaa et al. 2012). The latter authors, in particular, give estimates of the ISM characteristic turbulent velocities, defined as $v_{\rm turb} \equiv \sqrt{2}\,\sigma_{\rm turb}$ (linked to line broadening), in the central ∼10 kpc for two exemplary groups: $320 < v_{\rm turb} < 720$ km s^{-1} (NGC 5044) and $140 < v_{\rm turb} < 540$ km s^{-1} (NGC 5813). In order to compare the prediction of our CGG model with this observation, we calculate the 1D gas velocity dispersion along the line of sight l weighted by the emission measure, as

$$\sigma^2_{\rm turb} = \frac{\int \rho^2 (v_l - \bar{v}_l)^2 \, {\rm d}l}{\int \rho^2 \, {\rm d}l}, \qquad (5)$$

where the mean (emission-weighted) velocity $\bar{v}_l$ is typically close to zero, lacking large bulk motions.

In the (projected) circular region $0 < R < 5$ kpc, the time-average velocity dispersion is ∼200 km s^{-1} when the system is viewed along the outflow z-axis. In the phases where the AGN is more active, $\sigma_{\rm turb}$ can reach values as high as 400 km s^{-1}. Note that the outflow, with velocity often exceeding 10^4 km s^{-1}, contributes poorly to $\sigma_{\rm turb}$ because of the very low density. The gas turbulence becomes weaker at larger distances from the centre. In the ring $5 < R < 20$ kpc, $\sigma_{\rm turb}$ decreases to ∼60–100 km s^{-1}, while in the region $20 < R <$ 40 kpc, $\sigma_{\rm turb} \sim$ 40–70 km s^{-1}. One missing element of our models is the effect of cosmological merging and inflow, which may trigger additional turbulence, although more efficiently at large radii (>0.1 the virial radius, e.g. Vazza et al. 2011).

When the galaxy is observed along a line of sight perpendicular to the outflow direction (e.g. the x-axis), the mean central $\sigma_{\rm turb}$ has lower values, ∼100 km s^{-1}, with peaks about a factor of two larger. For the standard cooling-flow model presented in Section 3.1 we find instead $\sigma_{\rm turb} \lesssim 45$ km s^{-1}. This quantity is certainly not associated with turbulent motions, while it represents the steady radial inflow velocity due to a massive cooling flow.

We conclude that subrelativistic outflows are able to generate in the core the observed turbulent velocities, in the range $v_{\rm turb} \equiv \sqrt{2}\sigma_{\rm turb} \approx$ 100–400 km s^{-1}. The non-thermal pressure is generally a fraction of the thermal energy, around one-third ($E_{\rm turb}/E_{\rm th} \approx 0.2\,[v^2_{\rm turb,200}/T_7]$, where the turbulent velocity is expressed in units of 200 km s^{-1} and the gas temperature in units of 10^7 K).

5.2 Comparison with other AGN feedback scenarios

It is interesting to compare our purely mechanical feedback with other types of AGN heating processes. To our knowledge, very few investigations have focused on AGN feedback in ellipticals.[6] For example, Ciotti & Ostriker (2007) and Ostriker et al. (2010) have investigated a type of feedback triggered by AGN radiation (mainly Compton heating and radiation pressure, plus an approximation of a broad-line-region wind), through 1D hydrodynamic simulations. The best models have been analysed in detail by Pellegrini, Ciotti & Ostriker (2012) and compared with observations. The key feature of these models is the formation of a cold shell at $r \sim 1$ kpc, the evolution of which governs the whole quasar-like feedback heating (in order to be efficient, radiative feedback requires a very dense, optically thick, absorbing medium). We note that in 1D simulations a cold shell can form numerically under several circumstances, with or without AGN heating (see for instance the 'galactic drip'

[6] We refer the reader to G11a and G11b for comparisons with different AGN feedback models in other types of environment, such as galaxy clusters (Vernaleo & Reynolds 2006; Cattaneo & Teyssier 2007).

phenomenon described in Mathews & Brighenti 1997 and Brighenti & Mathews 2002). It is not clear how 1D calculations are able to follow the formation and evolution of the shell realistically. The subsonic, non-radial gas velocity appearing in multidimensional models tends to suppress this feature (Brighenti & Mathews 1997). The cold shell is also Rayleigh–Taylor unstable and should fragment in about a dynamical time, $\sim$ afew $\times\ 10^6$ yr. Another complication is the difficulty for hydrodynamic simulations in reproducing the real complexity of the observed multiphase ISM in the inner $<$ kpc (see Introduction).

Given these uncertainties, it seems more appropriate to compare our results with those presented in Novak et al. (2011), where the 2D version of the previous feedback scenario for an isolated elliptical galaxy is investigated. In these simulations conical outflows, representing broad-absorption-line (BAL) winds, are generated near the centre of the grid, making the computed scenario qualitatively similar to our models. Novak et al. (2011) found that the accretion process significantly changes in 2D, reducing the effectiveness of the feedback mechanism with respect to isotropic 1D models. They explored the effect of varying the mechanical efficiency, finding that an acceptable BH growth is attained when $\epsilon \gtrsim 10^{-4}$, consistent with the preferred values found in our work. About $10^{10}\,\mathrm{M}_\odot$ of stars form in Novak's ellipticals, almost independently of the wind efficiency, implying a mean star-formation rate of $\sim 0.8\,\mathrm{M}_\odot\,\mathrm{yr}^{-1}$. It would be interesting to estimate the central Balmer indexes (dependent on the star-formation history) and compare them with the available observations (Kuntschner et al. 2010).

Unfortunately, Novak et al. (2011) do not show azimuthally averaged temperature and density profiles, thus it is not possible to assess the effect of the AGN feedback on these key observable constraints. Nevertheless, together with our calculations, the results presented in Novak et al. (2011) corroborate the potential importance of bipolar outflows as a primary source of AGN feedback.

Debuhr, Quataert & Ma (2012) carried out 3D SPH simulations of AGN outflows driven by quasar radiation during a major merger. They noted that radiation pressure alone does not produce any substantial feedback, requiring an additional momentum kick with velocity $\sim 10^4\,\mathrm{km\,s}^{-1}$ (like BAL winds), similar to our best models. Large values of the optical depth are usually required to boost such fast outflows ($\tau \sim$ 5–10). A strong isotropic outburst produces a clear galactic outflow, drastically reducing the mass inside 3 kpc (two orders of magnitude). This is a typical feature associated with strong isotropic heating (either mechanical or thermal), which unbinds and shocks the central gas to unobserved levels in normal ellipticals. Bipolar mechanical outflows are instead gentler, capable of reproducing the observed anisotropic X-ray features as cavities (Fig. 3).

As a concluding remark, we note that the radiative feedback displays a strong impact on the ISM only in the presence of quasar-like objects, which are certainly rare in the local Universe, with a rapid decline below redshift $\sim$1.8 (Schneider et al. 2005).

5.3 Comparison with galaxy clusters and groups

After a systematic study of AGN outflow feedback, from cluster scales down to the galactic systems (Gaspari et al. 2009, 2011a,b, 2012), it is worth wrapping up and emphasizing the main similarities and differences.

Despite the very different environments of clusters, groups and ellipticals, purely mechanical AGN feedback, in the form of massive anisotropic outflows, is still able to suppress the cooling flow down to a factor $\lesssim$5–10 per cent. The self-regulation process is fundamental for preserving the cool-core structure in a state of quasi-thermal equilibrium.

In order to have proper self-regulation, AGN feedback seems to require mechanical efficiencies decreasing with halo mass: $\epsilon \sim 5 \times 10^{-3}$ (cluster), $\sim 8 \times 10^{-4}$ (group) and $\sim 3 \times 10^{-4}$ (isolated elliptical). We stress that this ϵ probably does not represent the actual efficiency. The accreted mass on the black hole may be lower, while the feedback power could be maintained at the same level by increasing the efficiency. Nevertheless, the trend of increasing efficiency with system mass could be real. In fact, the same mechanical feedback successful in massive clusters ($M_{\rm vir} \sim 10^{15}\,\mathrm{M}_\odot$) needs to work on a relatively less powerful regime in order to prevent core disruption in groups or galaxies ($\lesssim 4 \times 10^{13}\,\mathrm{M}_\odot$), which are less bound objects. Even with a lower ϵ, the feedback in lighter haloes has yet more dramatic consequences on the temperature and density profiles, with stronger outbursts easily perturbing the central region. An isolated galaxy is the exemplary case, in which single outflows of power $\sim 10^{44}\,\mathrm{erg\,s}^{-1}$ and $\epsilon = 3.3 \times 10^{-4}$ can eject gas outside the small system, stopping cooling for several tens of Myr. Applying a feedback 20 times stronger, as required for clusters, would eject the whole ISM and empty the galaxy for several Gyr. The physical reason for the linking of mechanical efficiency with the environment/potential well is unclear and needs to be clarified through future investigations. The fact that the most massive black holes reside at the centre of clusters (McConnell et al. 2011) could play a crucial role.

The cooling-flow problem in our simulations is solved through AGN outflows for more than 7–10 Gyr, despite the exact details of the feedback mechanism (cf. G11a and Gaspari et al. 2012). In the cluster calculations the resulting feedback was impulsive, with strong outbursts sometimes exceeding the Eddington power. Increasing the resolution leads to a higher outflow frequency (and lower powers), because the central inflowing material is able to accrete more easily along the direction perpendicular to the jet axis. The AGN outburst frequency is also correlated with the efficiency, e.g. in the group the outflow injection is almost continuous with a duty cycle around 0.8. The isolated galaxy is a slightly different case, because the absence of circumgalactic gas helps the feedback action, leading to mildly impulsive behaviour.

The galaxy simulation cgg-8em4 (Section 4) can be regarded as a convergence test of the best feedback group model in G11b. The increase in resolution is almost a factor of 2 and we find indeed consistent results. Cooling rates and profiles are similar, concordant with observational data. Also, the jet powers ($\sim$3–5 $\times\ 10^{44}\,\mathrm{erg\,s}^{-1}$) are similar, showing an analogous evolutionary pattern and frequency. It is worth noting that the jet active region is $R \times z \simeq 1 \times 1\,\mathrm{kpc}^2$ in the CGG model, while it is $1 \times 2\,\mathrm{kpc}^2$ in the group run presented in G11b. Therefore, a slightly longer jet does not alter the feedback properties (the same can be said for the width, as tested in previous models).

In all the best models the self-regulated outflow velocities are around $10^4\,\mathrm{km\,s}^{-1}$, with rarer events reaching several 10^4–$10^5\,\mathrm{km\,s}^{-1}$ in the strongest phases. The mean mass outflow rate decreases with the mass of the system: several tens $\mathrm{M}_\odot\,\mathrm{yr}^{-1}$ (cluster), few $\mathrm{M}_\odot\,\mathrm{yr}^{-1}$ (group), and $\lesssim 1\,\mathrm{M}_\odot\,\mathrm{yr}^{-1}$ (isolated galaxy). More massive and slower outflows usually show a higher piercing power, producing a narrow unidirectional channel. This is more evident in almost continuous feedback models, like galaxy groups or galaxies with CGG. However, the projected X-ray surface-brightness maps mask this narrow feature ($\sim$1 kpc) most of the time. Moreover, the turbulence generated by the feedback can easily alter and fragment the jet path, producing tiny bubbles. In contrast, relatively lighter

and faster outflows (still subrelativistic) thermalize the energy more efficiently, inflating big buoyant bubbles.

In the cluster regime the bubbles usually have a radius of a few tens of kpc, with emission-weighted temperatures slightly hotter than the ambient medium; the reduced power in groups and ellipticals produces more 'delicate' cavities (with radii of several and a few kpc, respectively), showing relatively cold rims and mild internal temperatures; the jump in $SB_{\rm X}$ is typically 20–40 per cent. In all three systems, different or fragmented jet outbursts also generate a series of weak shocks with Mach number 1.1–1.3, visible as faint ripples in the temperature and brightness profiles. Another fundamental feature they all have in common is the uplift of relatively cold and metal-rich gas, in particular during more powerful episodes, restoring lost potential energy and creating an asymmetrical distribution in the iron abundance maps (10–20 per cent contrast with the background).

The most successful models are those in which the accretion is linked to cold gas. Hot gas accretion, based on the original Bondi prescription, usually provides accretion rates one or two orders of magnitude lower, requiring very high mechanical efficiencies, $\epsilon \gtrsim 0.1$, in order to make the feedback effective. Moreover, its continuous nature poses serious doubts regarding the cyclic production of typical features, such as buoyant cavities. Linking the accretion to the cooling rate instead induces a natural self-regulation, with some kind of recursive cycle and peaks of activity. The success of the feedback is essentially independent of the drop-out parameters, such as $T_{\rm cut}$ (e.g. 2×10^4 or 5×10^5 K), the drop-out function (exponential or step) or the delay associated with the free fall of cold blobs. The simulations carried out in Gaspari et al. (2012), with the accretion traced only by the inflow in the nuclear region, confirm that the bulk of AGN fuelling is associated with the cold, and not the hot, phase (check $\dot{M}_{\rm acc}$ in Fig. 3), for which condensation is linked to jet-induced thermal instabilities.

ACKNOWLEDGMENTS

The software used in this work was in part developed by the DOE NNSA-ASC OASCR Flash Center at the University of Chicago. We acknowledge the NASA awards SMD-10-1609, SMD-11-2209 (Pleiades) and the CINECA awards HP10BPTM62, HP10BOB5U6 (SP6). Partial support for this work was provided by NASA under grant NNH09ZDA001N, issued through the Office of Space Sciences Astrophysics Data Analysis Program. We also thank J. de Plaa, E. Churazov and P. Sharma for helpful comments and the referee for a constructive report.

REFERENCES

Balbus S. A., 1988, ApJ, 328, 395
Balbus S. A., Soker N., 1989, ApJ, 341, 611
Baldi A., Forman W., Jones C., Kraft R., Nulsen P., Churazov E., David L., Giacintucci S., 2009, ApJ, 707, 1034
Balogh M. L., Babul A., Voit G. M., McCarthy I. G., Jones L. R., Lewis G. F., Ebeling H., 2006, MNRAS, 366, 624
Benson A. J., Bower R. G., Frenk C. S., Lacey C. G., Baugh C. M., Cole S., 2003, ApJ, 599, 38
Beuing J., Dobereiner S., Bohringer H., Bender R., 1999, MNRAS, 302, 209
Biller B. A., Jones C., Forman W. R., Kraft R., Ensslin T., 2004, ApJ, 613, 238
Binney J., Tabor G., 1995, MNRAS, 276, 663
Böhringer H., Werner N., 2010, A&AR, 18, 127
Booth C. M., Schaye J., 2009, MNRAS, 398, 53
Bregman J. N., Parriott J. R., 2009, ApJ, 699, 923
Bregman J. N., Miller E. D., Irwin J. A., 2001, ApJ, 553, L125
Bregman J. N., Miller E. D., Athey A. E., Irwin J. A., 2005, ApJ, 635, 1031
Bregman J. N., Fabian A. C., Miller E. D., Irwin J. A., 2006, ApJ, 642, 746
Brighenti F., Mathews W. G., 1997, ApJ, 490, 592
Brighenti F., Mathews W. G., 1998, ApJ, 495, 239
Brighenti F., Mathews W. G., 1999, ApJ, 512, 65
Brighenti F., Mathews W. G., 2002, ApJ, 573, 542
Brighenti F., Mathews W. G., 2003, ApJ, 587, 580
Brighenti F., Mathews W. G., 2006, ApJ, 643, 120
Brüggen M., Ruszkowski M., Hallman E., 2005, ApJ, 630, 740
Brüggen M., Heinz S., Roediger E., Ruszkowski M., Simionescu A., 2007, MNRAS, 380, L67
Bullock J. S., Kolatt T. S., Sigad Y., Somerville R. S., Kravtsov A. V., Klypin A. A., Primack J. R., Dekel A., 2001, MNRAS, 321, 559
Buote D. A., Lewis A. D., Brighenti F., Mathews W. G., 2003, ApJ, 594, 741
Buote D. A., Brighenti F., Mathews W. G., 2004, ApJ, 607, L91
Buson L. M. et al., 1993, A&A, 280, 409
Caon N., Macchetto D., Pastoriza M., 2000, ApJS, 127, 39
Cappellaro E., Evans R., Turatto M., 1999, A&A, 351, 459
Cappi M. et al., 2009, A&A, 504, 401
Cappi M., Giustini M., Tombesi F., 2011, in Ness J.-U., Ehle M., eds, The X-ray Universe 2011. ESA, Noordwijk, p. 51
Cattaneo A., Teyssier R., 2007, MNRAS, 376, 1547
Cattaneo A. et al., 2009, Nat, 460, 213
Churazov E., Forman W., Jones C., Böhringer H., 2000, A&A, 356, 788
Churazov E., Sunyaev R., Forman W., Böhringer H., 2002, MNRAS, 332, 729
Churazov E., Sazonov S., Sunyaev R., Forman W., Jones C., Böhringer H., 2005, MNRAS, 363, L91
Ciotti L., Ostriker J. P., 1997, ApJ, 487, L105
Ciotti L., Ostriker J. P., 2007, ApJ, 665, 1038
Ciotti L., D'Ercole A., Pellegrini S., Renzini A., 1991, ApJ, 376, 380
Colbert J. W., Mulchaey J. S., Zabludoff A. I., 2001, AJ, 121, 808
Crenshaw D. M., Kraemer S. B., George I. M., 2003, ARA&A, 41, 117
Croton D. J. et al., 2006, MNRAS, 365, 11
Dalla Vecchia C., Bower R. G., Theuns T., Balogh M. L., Mazzotta P., Frenk C. S., 2004, MNRAS, 355, 995
David L. P., Forman W., Jones C., 1991, ApJ, 380, 39
David L. P., Jones C., Forman W., Daines S., 1994, ApJ, 428, 544
David L. P., Jones C., Forman W., Vargas I. M., Nulsen P., 2006, ApJ, 653, 207
David L. P., Jones C., Forman W., Nulsen P., Vrtilek J., O'Sullivan E., Giacintucci S., Raychaudhury S., 2009, ApJ, 705, 624
David L. P. et al., 2011, ApJ, 728, 162
de Plaa J., Zhuravleva I., Werner N., Kaastra J. S., Churazov E., Smith R. K., Raassen A. J. J., Grange Y. G., 2012, A&A, 539, A34
Debuhr J., Quataert E., Ma C.-P., 2012, MNRAS, 420, 2221
Di Matteo T., Allen S. W., Fabian A. C., Wilson A. S., Young A. J., 2003, ApJ, 582, 133
Diehl S., Statler T. S., 2008a, ApJ, 680, 897
Diehl S., Statler T. S., 2008b, ApJ, 687, 986
Dong R., Rasmussen J., Mulchaey J. S., 2010, ApJ, 712, 883
Dubois Y., Devriendt J., Slyz A., Teyssier R., 2010, MNRAS, 409, 985
Dunn R. J. H., Fabian A. C., 2006, MNRAS, 373, 959
Dunn J. P. et al., 2010a, ApJ, 709, 611
Dunn R. J. H., Allen S. W., Taylor G. B., Shurkin K. F., Gentile G., Fabian A. C., Reynolds C. S., 2010b, MNRAS, 404, 180
Ellis S. C., O'Sullivan E., 2006, MNRAS, 367, 627
Eskridge P. B., Fabbiano G., Kim D.-W., 1995, ApJS, 97, 141
Fabian A. C., 1994, ARA&A, 32, 277
Fabian A. C., Rees M. J., 1995, MNRAS, 277, L55
Ferrarese L., Merritt D., 2000, ApJ, 539, L9
Ferrari F., Pastoriza M. G., Macchetto F., Caon N., 1999, A&AS, 136, 269
Ferreras I., Silk J., 2000, ApJ, 541, L37
Finoguenov A., Ruszkowski M., Jones C., Brüggen M., Vikhlinin A., Mandel E., 2008, ApJ, 686, 911

Fryxell B. et al., 2000, ApJS, 131, 273
Fukazawa Y., Botoya-Nonesa J. G., Pu J., Ohto A., Kawano N., 2006, ApJ, 636, 698
Gaspari M., Melioli C., Brighenti F., D'Ercole A., 2009, in Heinz S., Wilcots E., eds, AIP Conf. Ser. Vol. 1201, The Monster's Fiery Breath: Feedback in Galaxies. Am. Inst. Phys., New York, p. 309
Gaspari M., Melioli C., Brighenti F., D'Ercole A., 2011a, MNRAS, 411, 349 (G11a)
Gaspari M., Brighenti F., D'Ercole A., Melioli C., 2011b, MNRAS, 415, 1549 (G11b)
Gaspari M., Ruszkowski M., Sharma P., 2012, ApJ, 746, 94
Gastaldello F., Buote D. A., Temi P., Brighenti F., Mathews W. G., Ettori S., 2009, ApJ, 693, 43
Gebhardt K. et al., 2000, ApJ, 539, L13
Giacintucci S. et al., 2011, ApJ, 732, 95
Giovannini G., 2004, Ap&SS, 293, 1
Gitti M., O'Sullivan E., Giacintucci S., David L. P., Vrtilek J., Raychaudhury S., Nulsen P. E. J., 2010, ApJ, 714, 758
Gitti M., Brighenti F., McNamara B. R., 2012, Adv. in Astronomy, 2012, 1
Goudfrooij P., Hansen L., Jorgensen H. E., Norgaard-Nielsen H. U., 1994, A&AS, 105, 341
Graves G. J., Faber S. M., Schiavon R. P., 2009, ApJ, 698, 1590
Greggio L., 2005, A&A, 441, 1055
Guo F., Mathews W. G., 2010, ApJ, 712, 1311
Heckman T. M., Baum S. A., van Breugel W. J. M., McCarthy P., 1989, ApJ, 338, 48
Heinz S., Brüggen M., Friedman S., 2011, ApJS, 194, 21
Humphrey P. J., Buote D. A., 2006, ApJ, 639, 136
Humphrey P. J., Buote D. A., Gastaldello F., Zappacosta L., Bullock J. S., Brighenti F., Mathews W. G., 2006, ApJ, 646, 899
Igumenshchev I. V., 2006, ApJ, 649, 361
Irwin J. A., Sarazin C. L., Bregman J. N., 2002, ApJ, 570, 152
Jeong H. et al., 2009, MNRAS, 398, 2028
Jones C., Forman W., Vikhlinin A., Markevitch M., David L., Warmflash A., Murray S., Nulsen P. E. J., 2002, ApJ, 567, L115
Khosroshahi H. G., Jones L. R., Ponman T. J., 2004, MNRAS, 349, 1240
Kim D.-W., Fabbiano G., 2003, ApJ, 586, 826
King A. R., Pringle J. E., 2007, MNRAS, 377, L25
Kirkpatrick C. C., McNamara B. R., Cavagnolo K. W., 2011, ApJ, 731, L23
Krumholz M. R., McKee C. F., Klein R. I., 2005, ApJ, 618, 757
Krumholz M. R., McKee C. F., Klein R. I., 2006, ApJ, 638, 369
Kuntschner H. et al., 2010, MNRAS, 408, 97
Loewenstein M., 1989, MNRAS, 238, 15
Loewenstein M., Mathews W. G., 1987, ApJ, 319, 614
Loewenstein M., Mushotzky R. F., Angelini L., Arnaud K. A., Quataert E., 2001, ApJ, 555, L21
Macchetto F., Pastoriza M., Caon N., Sparks W. B., Giavalisco M., Bender R., Capaccioli M., 1996, A&AS, 120, 463
MacDonald J., Bailey M. E., 1981, MNRAS, 197, 995
Machacek M., Nulsen P. E. J., Jones C., Forman W. R., 2006, ApJ, 648, 947
Machacek M. E., Jerius D., Kraft R., Forman W. R., Jones C., Randall S., Giacintucci S., Sun M., 2011, ApJ, 743, 15
Malagoli A., Rosner R., Fryxell B., 1990, MNRAS, 247, 367
Mannucci F., Della Valle M., Panagia N., Cappellaro E., Cresci G., Maiolino R., Petrosian A., Turatto M., 2005, A&A, 433, 807
Martel A. R., Turner N. J., Sparks W. B., Baum S. A., 2000, ApJS, 130, 267
Mathews W. G., 1990, ApJ, 354, 468
Mathews W. G., 2009, ApJ, 695, L49
Mathews W. G., Baker J. C., 1971, ApJ, 170, 241
Mathews W. G., Brighenti F., 1997, in Arnaboldi M., Da Costa G. S., Saha P., eds, ASP Conf. Ser. Vol. 116, The Nature of Elliptical Galaxies, 2nd Stromlo Symposium. Astron. Soc. Pac., San Francisco, p. 405
Mathews W. G., Brighenti F., 2003, ARA&A, 41, 191
Mathews W. G., Brighenti F., 2008, ApJ, 685, 128
Mathews W. G., Loewenstein M., 1986, ApJ, 306, L7
Mathews W. G., Faltenbacher A., Brighenti F., Buote D. A., 2005, ApJ, 634, L137
Mathews W. G., Brighenti F., Faltenbacher A., Buote D. A., Humphrey P. J., Gastaldello F., Zappacosta L., 2006, ApJ, 652, L17
McConnell N. J., Ma C.-P., Gebhardt K., Wright S. A., Murphy J. D., Lauer T. R., Graham J. R., Richstone D. O., 2011, Nat, 480, 215
McCourt M., Sharma P., Quataert E., Parrish I. J., 2012, MNRAS, 419, 3319
McDonald M., Veilleux S., Mushotzky R., 2011, ApJ, 731, 33
McNamara B. R., Nulsen P. E. J., 2007, ARA&A, 45, 117
Mellier Y., Mathez G., 1987, A&A, 175, 1
Merloni A., Heinz S., 2008, MNRAS, 388, 1011
Moe M., Arav N., Bautista M. A., Korista K. T., 2009, ApJ, 706, 525
Morganti R., Holt J., Saripalli L., Oosterloo T. A., Tadhunter C. N., 2007, A&A, 476, 735
Mościbrodzka M., Proga D., 2008, ApJ, 679, 626
Mościbrodzka M., Proga D., 2009, MNRAS, 397, 2087
Nagino R., Matsushita K., 2009, A&A, 501, 157
Narayan R., Fabian A. C., 2011, MNRAS, 415, 3721
Narayan R., McClintock J. E., 2008, New Astron. Rev., 51, 733
Navarro J. F., Frenk C. S., White S. D. M., 1996, ApJ, 462, 563
Nesvadba N. P. H., Lehnert M. D., De Breuck C., Gilbert A. M., van Breugel W., 2008, A&A, 491, 407
Novak G. S., Ostriker J. P., Ciotti L., 2011, ApJ, 737, 26
O'Dea C. P. et al., 2008, ApJ, 681, 1035
O'Sullivan E., Giacintucci S., David L. P., Vrtilek J. M., Raychaudhury S., 2011a, MNRAS, 411, 1833
O'Sullivan E., Worrall D. M., Birkinshaw M., Trinchieri G., Wolter A., Zezas A., Giacintucci S., 2011b, MNRAS, 416, 2916
Oegerle W. R., Hill J. M., 2001, AJ, 122, 2858
Omma H., Binney J., Bryan G., Slyz A., 2004, MNRAS, 348, 1105
Ostriker J. P., Choi E., Ciotti L., Novak G. S., Proga D., 2010, ApJ, 722, 642
Parriott J. R., Bregman J. N., 2008, ApJ, 681, 1215
Pellegrini S., Ciotti L., Ostriker J. P., 2012, ApJ, 744, 21
Peterson J. R., Fabian A. C., 2006, Phys. Rep., 427, 1
Peterson J. R. et al., 2001, A&A, 365, L104
Peterson J. R., Kahn S. M., Paerels F. B. S., Kaastra J. S., Tamura T., Bleeker J. A. M., Ferrigno C., Jernigan J. G., 2003, ApJ, 590, 207
Piontek F., Steinmetz M., 2011, MNRAS, 410, 2625
Pizzolato F., Soker N., 2005, ApJ, 632, 821
Pizzolato F., Soker N., 2010, MNRAS, 408, 961
Pope E. C. D., 2007, MNRAS, 381, 741
Pope E. C. D., 2009, MNRAS, 395, 2317
Puchwein E., Sijacki D., Springel V., 2008, ApJ, 687, L53
Quataert E., Narayan R., 2000, ApJ, 528, 236
Randall S. W. et al., 2011, ApJ, 726, 86
Rasmussen J., Ponman T. J., 2009, MNRAS, 399, 239
Reale F., Rosner R., Malagoli A., Peres G., Serio S., 1991, MNRAS, 251, 379
Sanders J. S., Fabian A. C., Smith R. K., 2011, MNRAS, 410, 1797
Sansom A. E., O'Sullivan E., Forbes D. A., Proctor R. N., Davis D. S., 2006, MNRAS, 370, 1541
Sarazin C. L., Ashe G. A., 1989, ApJ, 345, 22
Sarazin C. L., White R. E., III, 1988, ApJ, 331, 102
Sarazin C. L., Irwin J. A., Bregman J. N., 2001, ApJ, 556, 533
Sarzi M. et al., 2006, MNRAS, 366, 1151
Sarzi M. et al., 2010, MNRAS, 402, 2187
Schneider D. P. et al., 2005, AJ, 130, 367
Sharma P., McCourt M., Quataert E., Parrish I. J., 2012, MNRAS, 2294
Shields J. C., 1991, AJ, 102, 1314
Sijacki D., Springel V., Di Matteo T., Hernquist L., 2007, MNRAS, 380, 877
Soker N., Pizzolato F., 2005, ApJ, 622, 847
Springel V., Di Matteo T., Hernquist L., 2005, MNRAS, 361, 776
Sutherland R. S., Dopita M. A., 1993, ApJS, 88, 253
Tamura T., Kaastra J. S., Makishima K., Takahashi I., 2003, A&A, 399, 497
Taylor G. B., Sanders J. S., Fabian A. C., Allen S. W., 2006, MNRAS, 365, 705
Temi P., Brighenti F., Mathews W. G., 2009, ApJ, 707, 890
Tombesi F., Cappi M., Reeves J. N., Palumbo G. G. C., Yaqoob T., Braito V., Dadina M., 2010a, A&A, 521, A57

Tombesi F., Sambruna R. M., Reeves J. N., Braito V., Ballo L., Gofford J., Cappi M., Mushotzky R. F., 2010b, ApJ, 719, 700
Tombesi F., Cappi M., Reeves J. N., Braito V., 2012, MNRAS, 422, 1
Tornatore L., Borgani S., Springel V., Matteucci F., Menci N., Murante G., 2003, MNRAS, 342, 1025
Trager S. C., Faber S. M., Worthey G., González J. J., 2000, AJ, 119, 1645
Tran H. D., Tsvetanov Z., Ford H. C., Davies J., Jaffe W., van den Bosch F. C., Rest A., 2001, AJ, 121, 2928
Trinchieri G. et al., 2008, ApJ, 688, 1000
Vazza F., Brunetti G., Gheller C., Brunino R., Brüggen M., 2011, A&A, 529, A17
Verdoes Kleijn G. A., Baum S. A., de Zeeuw P. T., O'Dea C. P., 2002, AJ, 123, 1334
Vernaleo J. C., Reynolds C. S., 2006, ApJ, 645, 83
Vikhlinin A., 2006, ApJ, 640, 710
Werner N., Zhuravleva I., Churazov E., Simionescu A., Allen S. W., Forman W., Jones C., Kaastra J. S., 2009, MNRAS, 398, 23
Xu H. et al., 2002, ApJ, 579, 600
Yoshida T., Habe A., Hattori M., 1991, MNRAS, 248, 630
Zanni C., Murante G., Bodo G., Massaglia S., Rossi P., Ferrari A., 2005, A&A, 429, 399

This paper has been typeset from a TEX/LATEX file prepared by the author.